TCF1 controls Treg functions that regulate inflammation, CD8 T-cell cytotoxicity, and severity of colon cancer

Khashayarsha Khazaie (Khazaie@mayo.edu)
Mayo Clinic
Abu Osman
University of Chicago
Bingyu Yan
Purdue University West Lafayette https://orcid.org/0000-0003-4429-8200
Ying Li
Mayo Clinic
Kevin Pavelko
Mayo Clinic https://orcid.org/0000-0001-7555-1315
Jasmin Quandt
University of Chicago
Abdulrahman Saadalla
Mayo Clinic
Mahendra Rathore
Mayo Clinic
Majid Kazemian
Purdue University
Fotini Gounari
University of Chicago https://orcid.org/0000-0003-2936-066X

Article

Keywords: T regulatory cells (Tregs), Tcf1, colon cancer

Posted Date: January 13th, 2021

DOI: https://doi.org/10.21203/rs.3.rs-136816/v1

Version of Record: A version of this preprint was published at Nature Immunology on August 12th, 2021. See the published version at https://doi.org/10.1038/s41590-021-00987-1.

Title

TCF1 controls T_{reg} functions that regulate inflammation, CD8 T-cell cytotoxicity, and severity of colon cancer.

Authors

Abu Osman[1,2,+], Bingyu Yan[3 +], Ying Li[4], Kevin Pavelko[1], Jasmine Quandt[2], Abdulrahman Saadalla[1], Mahendra Rathore[1], Majid Kazemian[3,5]*, Fotini Gounari[2]*, Khashayarsha Khazaie[1]*

[1] Department of Immunology, Mayo Clinic, Rochester, MN
[2] Department of Medicine, Section of Rheumatology, University of Chicago, Chicago, IL
[3] Department of Biochemistry, Purdue University, IN
[4] Division of Biomedical Statistics and Informatics, Mayo Clinic, Rochester, MN.
[5] Department of Computer Science, Purdue University, IN

[+] equally contributing authors
* co-corresponding authors

Abstract

TCF1 is essential for the development and function of T regulatory cells (T_{reg}s). However, how TCF1 regulates T_{reg} function in homeostasis or under pathogenic conditions is poorly understood. Here, we ablated TCF1 in T_{reg}s to elucidate its role in T_{reg} specification in healthy mice and mice with colon cancer. RNAseq revealed that TCF1-deficient T_{reg}s maintain their core transcriptional signature, but promote T-cell receptor, Tgfβ receptor, T_H17, and Wnt/β-catenin signaling pathways. Single-cell RNAseq identified central-memory-T_{reg}s with low *Klf2* or high *Mif* expression, which upon downregulation of TCF1 gained T_H17 characteristics and matured into *Maf* expressing effector T_{reg}s. Tcf1-deficient T_{reg}s exhibited enhanced suppression of T-cell proliferation and cytotoxicity but were compromised in controlling $CD4^+$ T-cell polarization and inflammation. In mice with polyposis, Tcf1-deficient T_{reg}s promoted inflammation and tumor growth. Thus, TCF1 differentially regulates T_{reg} control of T_H17 inflammation and T-cell cytotoxicity, and its action in T_{reg}s determines colorectal cancer outcome.

Introduction

Regulatory T-cells (T_{reg}s) are a heterogenous population of cells of thymic and extrathymic origins with diverse immune suppressive functions. Expression of the lineage-determining transcription factor Foxp3 is essential for maintaining T_{reg} identity [1, 2, 3], but is not sufficient to account for their substantial functional diversity [4]. In addition to FOXP3, T_{reg}s can express other transcription factors that are normally associated with T-helper cell functions, namely RORγt[5, 6, 7], GATA3[8, 9], or TBET[10, 11, 12]. More than half of gut-infiltrating T_{reg}s in healthy mice express RORγT[6, 7] and cMAF[13, 14, 15], and these T_{reg}s critically maintain immunotolerance and host microbe homeostasis. GATA3-expressing T_{reg}s are prevalent in the small intestine[6, 7, 8, 16], express HELIOS and ST2 (IL33 receptor), expand in response to IL-33[16, 17], and are highly T-cell suppressive[18, 19]. Both RORγt[6, 7]- and GATA3[8, 16, 20, 21]-expressing T_{reg}s produce high levels of IL-10 and suppress T_H2- and T_H17-mediated inflammation. They also accumulate in colon tumors, and have tumor-promoting properties[22, 23], although it is unlcear to what extent their functions are altered in the cancer setting.

Recent single-cell RNA sequencing (scRNAseq) studies have identified two transcriptionally distinct subpopulations of activated/effector-T_{reg}s (eT_{reg}s) in addition to central-memory-T_{reg}s (cT_{reg}s) [7, 24, 25]. One expresses elevated levels of RORC and its regulator c-Maf and the other expresses IKZF2/HELIOS, GATA3, and downstream ST2/IL33-receptor. The mouse RORγT$^+$ T_{reg}s are generated from naïve conventional CD4$^+$ T-cells (T_{conv}) after stimulation by bacteria antigens and also through interaction with the enteric nervous system [7, 24, 25]. The IKZF2/HELIOS T_{reg}s are mainly of thymic origin, although a subset of these that potentially originate from T_{conv} cells can convert to RORγt$^+$ T_{reg}s[25]. Analysis of T_{reg}s in humans also revealed several subpopulations of eT_{reg}s and cT_{reg}s[26]. T_{reg}s expand in response to inflammation and tumor growth. T_{reg} adapt to environmental challenges to re-establish homeostasis or drive pathogenic conditions, but the molecular underpinning of these responses at the single cell level is still poorly understood.

T_{reg}s expressing RORγT and IL17 have been described in fungal infections of mice[27] and were attributed with proinflammatory functions in humans[23, 28, 29]. In colorectal cancer (CRC) a notable subset of tumor-infiltrating

T_{reg}s express IL17, RORγT [23, 29], and high levels of β-catenin[30]. This subset is readily detectable in circulating blood of CRC patients but rapidly decline with surgical removal of the primary tumor [29, 30]. Expansion of RORγT$^+$ T_{reg}s in CRC is tumor dependent and coincides with suppression of T-cells, but overall loss of T_{reg} expression of IL10 and compromise of their anti-inflammatory properties[29, 30]. In mouse models of hereditary colon cancer T_{reg}s over express β-catenin, RORγT, and IL17, and promote tumor growth[23, 29, 31]. T_{reg}-specific ablation of RORγt attenuates inflammation and polyposis[23]. Using mouse models, we demonstrated that β-catenin increases chromatin accessibility at the *Rorc* locus and other genes associated with T_H17 inflammation to render T_{reg}s pro-inflammatory [30] (Quandt et al, Nature Immunology in press). These findings were corroborated by an independent report of T_{reg}s in multiple sclerosis, which express elevated expression of β-catenin, secret Ifnγ , and promote inflammation, but maintain their ability to suppress T-cells[32]. In total, these obserations indicate a pathogenic β-catenin and RORγT axis in T_{reg}s that alters T_{reg} functions, rendering them pro-inflammatory but highly T-cell suppressive in diseases such as cancer and autoimmunity. The contrast between the properties of RORγT$^+$ Tregs in health and disease is strinking and urges better understand of the molecular underpinning of pro-inflammatory RORγT$^+$ T_{reg}s.

TCF1 is the T-cell specific DNA binding partner of β-catenin[33, 34]. TCF1 interacts with FOXP3[35, 36] to repress the MAF-RORγ axis[37] and preserve T_{reg} suppressive functions. However, germline TCF1 deficiency induces premature expression of FOXP3 in double-positive thymocytes[38] and expands thymic T_{reg}s[39], suggesting a role in T_{reg} specification rather than maintaining T_{reg} identity. Here, we address how the loss of TCF1 post thymic-selection alters T_{reg} properties in healthy mice and in mice with polyposis. We report that T_{reg}s lacking TCF1 become activated and gain T_H17 properties while maintaining their core T_{reg} gene expression signature, molecular heterogeneity, and robust T_{reg} characteristics. Functionally, TCF1 deficiency compromises the ability of T_{reg}s to suppress T_H1 or T_H17 polarization of CD4 T-cells, but enhances their suppression of T-cell proliferation and antigen-specific cytotoxicity. T_{reg} specific deficiency of TCF1 increases tumor load and aggression in mice predisposed to polyposis. We conclude that TCF1 differentially controls independent T_{reg} suppressive functions, and that deregulation of this mechanism renders them pathogenic and tumor promoting in genetically susceptible hosts.

Results

TCF1 deficiency programs T_{reg}s for activation, T_H17 characteristics, and TGFβ signaling.

To understand how Tcf1 (encoded by *Tcf7*) alters T_{reg} properties, we generated mice double homozygous for the conditional $Tcf7^{fl/fl}$ (European Mouse Mutant Archive)[40] and $Foxp3^{Cre}$ alleles[41]. FACS analysis of mononuclear cells from the mesenteric lymph nodes (MLNs) of the $Foxp3^{Cre}Tcf7^{fl/fl}$ mice confirmed that TCF1 expression was lost in T_{reg}s **(Fig. S1a-b)** and not in conventional $CD4^+$ T-cells (T_{conv}s) **(Fig. S1c)**. We first performed bulk RNAseq analysis comparing purified T_{reg}s from pooled lymph nodes of 12-week-old $Foxp3^{Cre}Tcf7^{fl/fl}$ and control $Foxp3^{Cre}$ mice (n=3 independent biological replicates). We noted 1,090 upregulated genes (fold change >1.5 and FDR < 0.001), including *IL2ra* [42, 43], *Foxp3* [1, 44, 45], *Foxo1* [46, 47, 48, 49], *Tgfb1* [50, 51, 52], *Lef1* [36, 53], *Rara* [54, 55], and *Gata3* [8, 9], and 422 downregulated genes including *Ctla4*, *Ikzf2*/Helios, and *Gzmb* **(Fig. 1a)**. To identify pathways that are affected by TCF1, we performed gene set enrichment analysis (GSEA) on all Kegg pathways comparing transcriptomes of knockout and wildtype T_{reg}s (FDR<0.25; **Fig. 1b, Table S1**). TCF1-affected genes were not differentially enriched in core T_{reg} signature genes (**Fig. S1d**), suggesting that the T_{reg} core program is not compromised in Tcf1-deficient cells. Genes more highly expressed in TCF1-deficient T_{reg}s than in the control were strongly enriched in WNT signaling, MAPK signaling, T_H17 differentiation, IL17 signaling, TGFβ signaling, and T-cell receptor (TCR) signaling (**Fig. 1b**). The enhanced WNT signature could be the result of loss of TCF1-mediated transcription inhibition[34]. The most significantly enriched genes within the leading edge for WNT signaling included *Lef1*, *Lrp5*, *Gsk3b*, *Csnk1e*, *Csnk2a2*, *Ep300*, and *Rac1*; T_H17 differentiation genes included *Tgfb1*, *IL6ra*, *Rarα, Stat3*, *Ifngr2*, *Gata3*, and *Tbx21* as well as genes downstream of the TCR; TGFβ signaling genes included *Tgfb1*, *Smad3*, *Smad7*, and *Myc*; TCR signaling genes included *Nfatc1*, *2*, *3*, *Rela*, *Fos*, *Jun*, *Plk3r1*, *Akt1*, *Nfkb1*, *Kras*, and *Plcg1*. (**Fig. 1c**). Collectively, our data show that TCF1 deficiency affects large numbers of genes and modulates several pathways related to the activation, function, and polarization of T_{reg}s.

To confirm these data at the protein level, we next performed FACS analysis (**Fig. 2**). TCF1-deficient T_{reg}s had elevated ratios of multiple cell surface activation markers[56, 57] including CD69, ICOS, PD1, and $CD44^+CD62L^-$

(Fig. 2a). The *Foxp3*^{Cre}*Tcf7*$^{fl/fl}$ mice had higher T_{reg} to CD4 T-cell ratios, and higher frequency as well as absolute numbers of T_{reg}s in secondary lymphoid organs than the *Foxp3*^{Cre} mice **(Fig. 2b)**. However, fewer TCF1-deficient T_{reg}s expressed CD25 than TCF1-sufficient T_{reg}s **(Fig. 2b).** T_{conv} cells in the lymph nodes and spleens of *Foxp3*^{Cre}*Tcf7*$^{fl/fl}$ mice were more activated than in control *Foxp3*^{Cre} mice, in agreement with an earlier study[36] **(Fig. 2c)**. We also observed elevated frequencies of RORγt-expressing T_{reg}s in the MLN, spleen, small bowel, and colon, regardless of their expression of HELIOS **(Fig. 2d)**. TCF1-deficient T_{reg}s expressed higher levels of TGFβR1, TGFR2, and pSMAD2/3 **(Fig. 2e)**. In addition, pSTAT5 and pS6, a downstream target of mTORC1 activity, were more highly expressed in TCF1-deficient T_{reg}s **(Fig. 2e)**. This is notable because the high basal activity of mTORC1 is an *in vivo* feature of T_{reg}s[58, 59] (reviewed by Chapman and Chi[60]). In conclusion, our protein level data show that TCF1 deficiency results in the activation of core T_{reg} and T_H17 signatures, consistent with the RNA data.

Single-cell transcriptomics delineate distinct T_{reg} subpopulations in the mesenteric lymph nodes.

To better understand how TCF1 regulates T_{reg} properties and possible relevance to colon cancer, we performed scRNAseq of T_{reg}s from MLNs of 5.5-month-old mice with four different genotypes (n=2 replicates per genotype): *Foxp3*^{Cre}*Tcf7*$^{fl/fl}$ and its control *Foxp3*^{Cre} mice, the polyposis prone *Apc*$^{\Delta 468}$ mice and control WT *C57BL/6J (B6)* mice. We enriched T_{reg}s to over 90% purity, using the untouched magnetic bead purification of $CD4^+$ T-cells followed by positive selection for CD25 (Miltenyi) (**Fig. S2**), and subjected them to scRNAseq using the 10X genomics platform. An unbiased integrative analysis across all four genotypes after regression for potential artifacts using the seurat platform[61] resulted in 14,487 cells grouped into 10 major subpopulations on UMAP projection (**Fig. 3a**, **Table S2**; see **Methods**). These subpopulations were annotated according to the most salient identified cell marker (**Fig. 3b**). We identified three clusters of T_{reg}s with activated/effector characteristics (eT_{reg}s), and annotated them as Maf, Ikzf2, and Mif based on their high expression of the corresponding genes. The Maf cluster had the highest expression of *Maf* as well as *S100a4*, *Rorc*, *Hif1a*, *Icos*, and *Rorα* **(Fig. 3b,c; S3a)**. The Ikzf2 cluster had the highest expression of *Ikzf2*/Helios as well as *Rora* , and *Gata3*, *IL7r*, and *Klrg1*, and the second highest expression of *Maf* and *Icos* **(Fig. 3b,c; Fig. S3a)**. HELIOS is a member of the IKAROS transcription factor family that regulates several T_{reg} suppressive functions[62] and is preferentially but

not exclusively expressed by thymus-derived naïve/cT$_{reg}$s[63]. The Ikzf2 cluster was enriched for *Gata3*-expressing T$_{reg}$s, which are largely thymus derived and have strong IL10-dependent anti-inflammatory properties important for maintaining gut homeostasis [16, 64]. The first two of these clusters have been described earlier as the RORγT^{+} and the HELIOS^{+} subsets of T$_{reg}$s[25] in mice, or as nonlymphoid T-cell like (nLT) T$_{reg}$s in mice and eT$_{reg}$s in humans[26]. The Mif (macrophage migration inhibitory factor) cluster has not been previously described, and could represent an early stage of pTreg differentiation or T-follicular suppressor T$_{reg}$s[65, 66]. MIF is the receptor for CXCR2 and CXCR4[67, 68] and regulates TLR4 expression and TCR signaling[69]. Of note, CXCR4 is a key chemokine for attracting extrafollicular T-lymphocytes[70] and plasmablasts[71, 72] and for demarcating germinal center dark and light zones[73]. MIF plays an important role in B-cell maturation and secretion of IgA in the gut [74, 75, 76], reviewed in [77]. The Mif cluster had high expression of activation markers *Nr4a1*(NUR77), *Tnfrsf9*/4-1bb, and *Hif1a* relative to the other clusters **(Fig. 3b).** It also expressed *Maf*, *Rorc*, and *Gata3* but less than the other two eT$_{reg}$ clusters. To obtain insight into the function of each subpopulation, we performed gene ontology pathway analysis on the genes upregulated in each cluster when compared to others using Metascape[78] (**Fig. 3d**). Genes upregulated in Maf and Ikzf2 clusters represented pathways associated with lymphocyte activation, immune response, negative regulation of immune system process, positive regulation of cytokine production, and high apoptotic signaling; by comparison, genes upregulated in the Mif cluster represented fewer pathways, the most outstanding one being regulation of response to cytokine stimulus **(Fig. 3c).**

Five other clusters (Klf2^{-}, Klf2^{+}, Klf2^{++}, Ncoa3) expressed naïve/central-memory markers (cT$_{reg}$s), comparable to the earlier descriptions of human central T$_{reg}$ (cT$_{reg}$)[26]. Three of these cT$_{reg}$ clusters were named by their relative expression of Kruppel-like Factor 2 (*Klf2*) as Klf2^{-}, Klf2^{+}, and Klf2^{++} **(Fig. 3a-c)**. *Klf2* is highly expressed by early thymic emigrants (ETE) [79, 80]. The Klf2^{++} cluser expressed other ETE markers including *S1pr1*[81, 82, 83], *Sell* (L-selectin/CD62L)[84], and *Igfbp4* [85]. KLF2 [86] and S1PR1[87] are involved in T$_{reg}$ migration to and establishment of immunological tolerance by naïve T$_{reg}$s in secondary lymphoid organs [86], and IGFBP4 blocks signaling by insulin-like growth factor and inhibits extrathymic induction of T$_{reg}$s[88]. The Klf2^{-} cluster stood out from the rest by its low expression of *Klf2* and ETE markers (**Fig. 3b**). Since Klf2^{-} and Klf2^{++} were the two largest T$_{reg}$ subpopulations (**Fig. 3a**), we directly compared their upregulated genes and identified the 20 most enriched pathways using Metascape[78]. The most significantly enriched pathways of the Klf2^{++} cluster included T-cell migration and

leukocyte cell-cell adhesion **(Fig. 3e)**. By contrast, T_{reg}s of the Klf2^{-} cluster were enriched for T_H17 cell differentiation, IgA production, and cytokine production **(Fig. 3e)**, indicating response to microbial antigens. Both clusters were enriched for leukocyte activation and immune response pathways, indicative of T_{reg} function within the secondary lymphnodes **(Fig. 3e)**. The Ncoa3 cluster expressed low to intermediate levels of *Klf2*, but was unique in its high expression of *Ncoa3*, a nuclear co-activator partner of arylhydrocarbone receptor[89, 90] and estrogen receptor alpha[91], as well as relatively high expression of *Notch2* **(Fig. 3b)**. The potential distinct function of this subpopulation is currently unknown. Although small, the Ifn subpopulation was conspicuous by its expression of multiple interferon response genes including *Stat1*, *Ifit1*, *Ifit3*, *Ifit1bl1*, and *Ifit3b* **(Fig. 3b,c).** Functionally, genes upregulated in this cluster were enriched in response to type-1 interferon, response to *Ifnγ*, and regulation of innate immune response (**Fig. 3d**). The Vsp8 cluster shared cT_{reg} expressed genes, except for the strong expression of *Vps8*, a subunit of the CORVET complex that coordinates lysosome fusion with endosomes[92, 93] **(Fig. 3a,b,d)**. The remaining cluster, namely Cd63, was spatially isolated from the other T_{reg} clusters, and is likely not to be T_{reg}s because of its expression of myeloid cell makers and low to undetectable expression of the core T_{reg} transcript[36, 42, 94] *Izumo1r* (FOLR4) **(Fig. 3a,b)**.

These analyses corroborate and earlier findings that indicate the existence of two eTreg and multiple cTreg clusters in mice, and further define a new Mif cluster with T-follicular suppressor classificataions and a novel Ifn cluster with narrow expression of interferon response genes. We classify the remaining cTreg clusters with respect to their relative expression *Klf2*, the significance of which becomes more obvious with our velocity analysis of the pseudotime trajectory of the clusters relative to the eTreg clusters, as described below.

TCF1-deficient and sufficient T_{reg}s show distinct effector functions.

To better understand the function of Tcf1 in T_{reg}s, we focused on scRNAseq data from *Foxp3^{Cre}Tcf7$^{fl/fl}$* T_{reg}s and control *Foxp3^{Cre}* T_{reg}s. Side-by-side comparison of UMAP projections did not reveal any noticable change in the numbers or cellular contents of the T_{reg} clusters with ablation of *Tcf7* (**Fig. 4a**). The quantitative analysis of the T_{reg}s in each cluster further coroborated similar cellularities across the two genotypes (**Fig. 4a, right panel**). To identify genes that are regulated by Tcf1, we directly compared the expression profiles of Tcf1-deficient to Tcf1-sufficient cells in each cluster (**Fig. 4b**; see **Table S3** for full data). Several genes were broadly elevated across

all TCF1-deficient T_{reg} clusters including *Dnaja1* that ecodes a heatshock protein cochaperone, and *Erdr1* a bacteria-sensitive secreted apoptic factor [95, 96] (**Fig. 4b** and **Fig. S4**). Others were uniformly downregulated, such as *Igfbp4*, an inhibitor of insulin-like growth factor receptor signalling [88](**Fig. 4b** and **Fig. S4**). Cells lacking TCF1 had elevated expression of *Maf* across all T_{reg} clusters with the exception of $Klf2^{+}$ and Ifn clusters, and elevated *Hsph1* in all but the Ncoa3 cluster (**Fig. 4b-c**). cMAF is essential for the generation of $ROR\gamma T^{+}$ T_{reg}s [13, 14, 15], and is negatively regulated by TCF1[37]. *Hsph1* encodes a heat shock protein that marks T_{reg} activation and is important for suppressive functions [97, 98]. Other genes with strongly elevated expression in the Maf and Ikzf2 clusters, and their potential precursors the $Klf2^{-}$ and Ncoa3 clusters, included *CCR9*, that encodes a gut tropic chemokine receptor which is essential for T_{reg} regulation of T_H17 inflammation [99, 100], and fibrinogen-like-protein-2 (*Fgl2*), a downstream target of TIGIT and an indispensable molecule for T_{reg} suppression of autoimmunity [101] (**Fig. 4b-c**). Enhanced expression of the gut-associated intergrin *Itgae*/CD103/αE-integrin was limited to the $Klf1^{-}$ and Maf clusters (**Fig. 4b**). The Ifn cluster was exceptional in showing the least change with the ablation of TCF7, except for *Dnaja1* (**Fig. 4b**) and *Erdr1* (**Fig. S4**). The intercluster relations were highly stable across all mouse genotypes analysed (**Fig. S3b**) and did change with the ablation of TCF1 in T_{reg}s.

To gain further insight into the function of TCF1, we performed GSEA (Stubbington) comparing TCF1-deficient and sufficient cells in each T_{reg} cluster. Lack of TCF1 had minimal effects on the core T_{reg} program (**Fig. 4d** with representative GSEA plot shown in **Fig. 4e**) consistent with our observation from bulk RNAseq (**Fig. S1d**). TCF1 deficiency broadly enhanced the expression of T_H17 (**Fig. 4d**) and/or IL17 (**Fig. 4f**) program genesets across T_{reg} clusters, using independent Stubbington and Kegg pathway module scores. The Vps8 cluster was exeptional in having highly-induced T_H1 signaling along with T_H17 signature, raising speculation that this cluster may be an intermediate to pathogenic T_H17 cells that co-express T_H1 and T_H17 cytokines [102, 103] (**Fig. 4d**). Collectively, these findings are compatible with loss of TCF1 resulting in the broad activation and gain of T_H17 properties by T_{reg}s, with the Maf cluster exhibiting the strongest change in gut homing potential and the Vsp8 cluster potentially differentiating into T_{eff} cells.

To determine the intercluster relations and how these may change with the loss of Tcf1, we overlaid RNA velocity vectors on the UMAP projection of T_{reg}s (**Fig. 4g**). RNA velocity predicts the future state of the cells using

unspliced and spliced mRNAs from scRNAseq data[104]. The velocity vectors suggested that the Maf T_{reg} cluster mainly derives from the Mif cluster, but to some extent also from the Ikzf2 and therefore indirectly from two cT_{reg} clusters, the $Klf2^{-}$ and Ncoa3. The lack of relation of the Mif cluster to cT_{reg} clusters indicated a potential extrathymic origin (**Fig. 4g**). This finding is compatible with the notion that $Ror\gamma t^{+}$ T_{reg}s, which are enriched in the Maf cluster, are extrathymically generated by bacterial stimulation of $CD4^{+}$ T_{conv} cells[7, 24, 25, 42, 105]. The Ikzf2 cluster derived from the $Klf2^{-}$ and Ncoa3 cT_{reg} clusters (**Fig. 4g**). These findings are compatible with earlier reports that the Ikzf2/$Helios^{+}$ T_{reg}s are largely of thymic origin, and capable of converting to $Ror\gamma t^{+}$ T_{reg}s but with relatively lower efficiency than $CD4^{+}$ T_{conv} cells [25]. The Vsp8 cluster vectors pointed away from all other T_{reg} clusters, in agreement with their potential differentiation into T_{eff} cells. Other inter-relations between the cT_{reg} clusters such as Ncoa3 with $Klf2^{-}$ and $Klf2^{++}$ with Ifn suggest plasticity and/or sequential stages of maturation of the cT_{reg}s.

The above findings were supported by scRNA analysis of T_{reg}s from WT and polyposis ridden $Apc^{\Delta 468}$ mice . T_{reg} clusters and relative frequencies of cells within each cluster did not change with polyposis in $Apc^{\Delta 468}$ mice (**Fig. S5a**; **Table S4**). The two activated Maf and Ikzf2 eT_{reg} clusters had lower expression of *Tcf7* as compared with the cTreg clusters, suggesting that T_{reg} activation requires downregulation of TCF1 (**Fig. S5b**). However, there were differences in gene expression between T_{reg}s from polyposis and WT mice. Expression of *Maf* was enhanced in the Maf cluster, *Jund* and *Tgfb1* were stronger in the $KLf2^{-}$ cluster, and *Jund* and *Soc3* were elevated in the $KLF2^{++}$ T_{reg} clusters of polyposis mice as compared to WT mice (**Fig. S5c&d**). *JunD*, encodes an AP1 transcription factor that is activated downstream of the TCR [106, 107], *Socs3*, encodes a major regulator of IL-23-mediated STAT3 phosphorylation and T_H17 generation [108], and *Lag3*, encodes a ligand for major histocompatibility complex class II (MHC-II) [109, 110] that is a critical mediator of immune suppression by T_{reg}s [111, 112]. Therefore, these transcriptional changes are compatible with activation of select cTreg clusters and enhanced immune suppressive activity of the *Maf* eTreg cluster during polyposis. Velocity analysis revealed similarities conserved intercluster relations among T_{reg}s of polyp-ridden and healthy mice. One possible exception was the enhanced differentiation of T_{reg}s from the Ikzf2 to the Maf cluster in polyp-bearing mice $Apc^{\Delta 468}$ mice relative to healthy WT control mice (**Fig. S5e**). Collectively, these findings are consistent with the activation and enhanced differentiation of Maf cluster T_{reg}s in polyposis relative to WT mice. The changes introduced in T_{reg}s by polyposis are similar to those caused by the loss of TCF1 in T_{reg}s of healthy mice.

TCF1-deficient T_{reg}s suppress viral antigen-specific $CD8^+$ T-cell cytotoxicity and T-cell proliferation.

T_{reg} suppression of $CD8^+$ T-cell cytotoxicity is TGFβ dependent [51, 52, 113]. Given their activated expression profile, preservation of the core T_{reg} signature, and the enhanced TGFβ signature, we predicted that TCF1-deficient T_{reg}s would efficiently suppress $CD8^+$ T-cell cytotoxic activity. To test this, we compared *in vivo* responses of *Foxp3^{Cre}Tcf7$^{fl/fl}$* and control *Foxp3^{Cre}* mice to Theiler's murine encephalomyelitis virus (TMEV). Infection with TMEV in H-2D^b mice results in an acute phase viremia that leads to the expansion of an immunodominant virus-specific $CD8^+$ T-cell response that peaks on day 7 post infection[114, 115]. Viral antigen-specific $CD8^+$ T-cell activity can be quantified by specific lysis of antigen pulsed splenocytes in the infected mice. We measured the relative effectiveness of T_{reg}s in suppressing this activity by comparing cell lysis in *Foxp3^{Cre}Tcf7$^{fl/fl}$* and *Foxp3^{Cre}* mice at the peak of the $CD8^+$ T-cell response. On day 7 post infection, mice received TMEV-$VP2_{121-130}$ pulsed and control unpulsed splenocytes, each labelled with a different intensity of CFSE **(Fig. 5a)**. Lysis of transferred cells was measured in the spleen four hours after transfer. As control, we transferred antigen pulsed aand unplulsed cells in naïve mice that had not been vaccinated. Antigen specific lysis of the pulsed cells was calculated after normalizing for nonspecific cell death in naïve mice. In parallel, to confirm that the $VP2_{121-130}$-specific $CD8^+$ T-cells were regulated in a TGFβ-dependent manner, we treated a separate group of mice from the day of infection with a small molecule inhibitor of TGFβR1 signaling that blocks phosphorylation of SMAD (LY3200882, Eli Lilly; kindly provided by Dr. Alexandra Vitko Lucs) or with vehicle as control. The infected *Foxp3^{Cre}Tcf7$^{fl/fl}$* mice lysed significantly fewer of the $VP2_{121-130}$ pulsed splenocytes than the *Foxp3^{Cre}* mice (~21% versus ~56% converted, $p< 0.0001$ Student t-test) **(Fig. 5b,c).** Treatment of mice with the LY3200882 inhibitor abrogated this difference, and increased the killing of $VP2_{121}$ pulsed splenocytes in *Foxp3^{Cre}Tcf7$^{fl/fl}$* mice to over 55% (**Fig. 5b,c)**. Our data suggest that the T_{reg}-specific loss of TCF1 in *Foxp3^{Cre}Tcf7$^{fl/fl}$* mice augments the suppression of anti-viral $CD8^+$ T-cell response. Mechanistically, the enhanced suppressive activity of *Foxp3^{Cre}Tcf7$^{fl/fl}$* T_{reg}s can be related to TGFβR1 signaling signaling as it was abrogated with LY3200882 a small molecule inhibitor of TGFβR1 signaling. These differences can be accounted for by enhanced TGFβ-dependent inhibition of $CD8^+$ T-cell cytotoxicity in mice.

To further assess the mechanisms of $CD8^+$ T-cell suppression, we monitored the fate of viral antigen-specific $CD8^+$ T-cells in the same mice using $VP2_{121-130}$ tetramers. TMEV infection of *Foxp3^{Cre}* mice triggered the expansion of $VP2_{121-130}$-specific $CD8^+$ T-cells nearly 14 fold from the steady-state frequency of 0.07% to almost 1% (p=0.004) of total $CD8^+$ T-cells at the peak of response to TMEV. This expansion was less than half in the infected *Foxp3^{Cre}Tcf7$^{fl/fl}$* mice, showing significant difference with baseline (p= 0.004) and with the expansion of the specific $CD8^+$ T-cells in mice with TCF1-deficient T_{reg}s (p=0.016). Thus, the proliferation of $VP2_{121-130}$-specific $CD8^+$ T-cells was more strongly suppressed in *Foxp3^{Cre}Tcf7$^{fl/fl}$* mice than in the *Foxp3^{Cre}* mice **(Fig. 5d)**. To independently validate the inhibition of T-cell proliferation by TCF1-deficient mice, we performed *in vitro* proliferation inhibition assays **(Fig. 5e)**. FACS purified $CD4^+CD25^+YFP^+$ $Foxp3^{Cre}$ T_{reg}s were cocultured with an equal number of purified naïve $CD4^+CD25^-$ T-cells and then stimulated with allogeneic splenocytes and αCD3. The Tcf1-deficient T_{reg}s exhibited stronger suppressive activity than TCF1-sufficient T_{reg}s ($p<0.05$; Student T-Test) **(Fig. 5f,g)**. Together, our data show that TCF1 deficiency augments the ability of T_{reg}s to suppress $CD8^+$ T-cell cytotoxicity and inhibit T-cell proliferation.

TCF1-deficient T_{reg}s fail to suppress T_H1 or T_H17 polarization of $CD4^+$ T_{conv} cells.

Inflammation requires $CD4^+$ T-cell help and we therefore compared Tcf1-deficient and sufficient T_{reg}s for their ability to suppress polarization of naïve $CD4^+$ T-cells to T_H1 or T_H17 type cells. For the *in vitro* assays, we stimulated splenocytes from *Foxp3^{Cre}Tcf7$^{fl/fl}$* mice and *Foxp3^{Cre}* mice with αCD3 under T_H1[116, 117, 118] **(Fig. 6a)** or T_H17[119, 120] **(Fig. 6d)** polarization conditions. We evaluated polarization by intracellular staining for Ifnγ or IL17. *Foxp3^{Cre}Tcf7$^{fl/fl}$* splenocytes were significantly more effective than the *Foxp3^{Cre}* splenocytes in T_H1 **(Fig. 6b)** (~25% versus ~10% converted, $p<0.0004$) or T_H17 **(Fig. 6e)** (~20% versus ~5% converted, $p< 0.0003$) polarization, suggesting a failure of *Foxp3^{Cre}Tcf7$^{fl/fl}$* T_{reg}s to control T_H cell polarization. To further validate this finding, we repeated the assay with purified $CD4^+$ T-cells from WT mice and purified T_{reg}s from *Foxp3^{Cre}Tcf7$^{fl/fl}$* or *Foxp3^{Cre}* mice. Tcf1-deficient T_{reg}s were consistently less effective in suppressing the polarization of T_{conv} cells to T_H1 **(Fig. 6c)** (~16% versus ~8% converted, $p < 0.002$) or T_H17 **(Fig. 6f)** (~17% versus ~9% converted, $p < 0.001$).

Next we assessed our findings in an *in vivo* setting using well established conditions that elicit T_H1 or T_H17 immunity in mice. Mice infected with TMEV mount a robust T_H1 response that promotes viral-specific $CD8^+$ T-cell cytolytic activity. We therefore infected mice with TMEV and after seven days isolated and re-stimulated mononuclear cells from spleen or MLNs with PMA/ionomycin/Golgistop **(Fig. 6g)**. Expression of Ifnγ by $CD4^+$ and $CD8^+$ T-cells was significantly higher in *Foxp3^{Cre}Tcf7$^{fl/fl}$* mice than in control *Foxp3^{Cre}* mice **(Fig. 6h,i)** (CD4: MLN 6% versus 3%, p <0.04 & spleen 20% versus 13% p<0.001, CD8: MLN 27% versus 14% p<0.003 & spleen 47% versus 32% p<0.001), indicating poor control of T_H1 polarization in mice with Tcf1-deficient T_{reg}s. To induce T_H17 polarization we followed a previously published protocol where intraperitoneal (*i.p.*) injection of αCD3 activates T_H17 polarization in the small bowel[121]. We injected mice *i.p.* with αCD3 and three days later quantified the expression of IL17 by CD4 T-cells in the small bowel by FACS **(Fig. 6j).** Injection of antibody produced significantly more IL17-expressing CD4 T_{eff} cells in *Foxp3^{Cre}Tcf7$^{fl/fl}$* mice than in control *Foxp3^{Cre}* mice (p< 0.01), indicating poor control of T_H17 polarization in mice with Tcf1-deficient T_{reg}s **(Fig. 6k)**. Collectively, our data show that TCF1-deficient T_{reg}s are compromised in their ability to suppress T_H1 and T_H17 polarization *in vitro* and *in vivo*.

TCF1-deficient T_{reg}s promote inflammation and tumor growth in polyposis-prone *Apc^{Δ468}* mice.

To assess the tumor-promoting properties of TCF1-deficient T_{reg}s, we crossed the *Foxp3^{Cre}Tcf7$^{fl/fl}$* and control *Foxp3^{Cre}* mice to the polyposis-prone *Apc^{Δ468}* mice [122], and generated two new compound mutant mouse strains: the TCF1 defective *Apc^{Δ468}Foxp3^{Cre}Tcf$^{fl/fl}$* mice and control *Apc^{Δ468}Foxp3^{Cre}* mice. At 5.5 months of age, the TCF1-defective mice had significantly more colon polyps than control mice (12% versus 4% p<0.0001) **(Fig. 7a)**, but similar numbers of polyps in the small bowel **(Fig. 7b)**. Nuclear β-catenin staining revealed that *Apc^{Δ468}Foxp3^{Cre}Tcf$^{fl/fl}$* mice had high incidence of pre-invasive colon tumors **(Fig. 7c)** and small bowel tumors **(Fig. 7d)** while these were rare in control *Apc^{Δ468}Foxp3^{Cre}* mice**.** The pre-invasive lesions were defined by the accumulation of abberant epithelial cells at the submucoal boundary **(Fig. 7e)**, in contrast to their accumulation at the luminal boundary of benign polyps in Tcf1-sufficient mice **(Fig. 7f)**.

Colon polyps of *Apc*$^{\Delta 468}$*Foxp3*^{Cre}*Tcf*$^{fl/fl}$ mice had significantly higher densities of Gr1^{+} cells than the polyps of *Apc*$^{\Delta 468}$*Foxp3*^{Cre} mice (116 per FOV versus 62 per FOV ; p< 0.0001) (**Fig. 7g,h)**, as did the small bowel polyps of *APC*$^{\Delta 468}$*Foxp3*^{Cre}*Tcf*$^{fl/fl}$ mice (13.5 per FOV) versus *Apc*$^{\Delta 468}$*Foxp3*^{Cre} mice (8.5 per FOV; p< 0.02) (**Fig. 7i,j**). The tumor-distant healthy tissues also had higher densities of Gr1^{+} cells in the *Apc*$^{\Delta 468}$*Foxp3*^{Cre}*Tcf*$^{fl/fl}$ mice than the *Apc*$^{\Delta 468}$*Foxp3*^{Cre} mice (colon: 1.2 versus 0.4 per FOV; p<0.009 and small bowel: 2 versus 1 per FOV; p<0.01) (**Fig. 7g-j)**. Together, these findings establish that loss of Tcf1 in T_{reg}s leads to gain of pro-inflammatory and tumor-promoting properties in the colon of mice with genetic predisposition to polyposis.

Discussion

Our findings highlight the role of TCF1 in regulating multiple independent mechanisms by which T_{reg}s fine tune immunity. TCF1 deficient T_{reg} gained a “split personality” similar to that observed with T_{reg}s in CRC[123]. While compromised in suppressing inflammation they became more activated and potently hindered proliferation and antigen specific cytotoxicity of effector T-cells, T-cell functions relevant to tumor rejection. In mice genetically predisposed to polyposis, TCF1-deficient T_{reg}s exhibited tumor-promoting properties demonstrating the significance of TCF1 signaling in T_{reg}s to the outcome of CRC. Together these findings demonstrate that TCF1 coordinates independent suppressive properties of T_{reg}s, which when deregulated in cancer can favor tumor growth.

Bulk RNA seq showed that TCF1-deficient T_{regS} have upregulated core T_{reg} signature genes including Foxp3, IL2rα, Foxo1, Gata3, and Tgfβ1, and enhancesd Wnt, TGFβ, T_H17, IL17, MAPkinase, and TCR signaling. Our scRNAseq analysis demonstrated that these changes were caused by altered gene expression within molecularly conserved T_{reg} clusters, rather than gain or loss of T_{reg} subsets. We identified two transcriptionally distinct subpopulations of eT_{reg}s marked by high expression of *cMaf* or *Ikzf2* in addition to several clusters of cT_{reg}s, consistent with recent scRNAseq studies[7, 24, 25]. The cMaf cluster had the strongest expresioon of *Rorc*. Since expression of *Rorc* by T_{reg}s is bacterial dependent[7], the cMaf cluster is likely to have originated from naïve conventional CD4^{+} T-cells (T_{conv}) through interaction with the gut microbiota. Consistently, our velocity analysis

indicated that this cluster largely derives from the Mif cluster, a less activated T_{reg} cluster which does not relate to the other cTreg clusters. Ikzf2 encodes HELIOS, which serves to enhance T_{reg} fitness[62], and when expressed by naïve T_{reg}s can be an indication for their thymic origin [63]. It is reported that the Ikzf2 cluster of T_{reg}s can convert to RORγT^{+} T_{reg}s albeit less efiiciently than conventional CD4^{+} T-cells [25]. Accordingly, our velocity analysis indicated that the Ikzf2 cluster derives mainly from *Klf2* low expressing cTreg clusters and contributes to the Maf cluster. The Ikzf2 cluster was enriched for the expression of *Gata3* and the downstream *St2*/IL33-receptor. We found that ablation of *Tcf7* upregulates expression of *cMaf* and augments the T_H17 signaling pathway in both clusters, but most prominently in the cMaf cluster. This is compatible with earlier findings that TCF1 suppresses expression of *cMaf* and *Rorc* [36, 37, 124]. It is also consistent with gain of proinflammatory properties by the cMaf cluster and the contribution of both extrathymic and thymic derived T_{reg}s to this cluster. Analysis of the WT aand *Apc*$^{\Delta 468}$ polyposis mice revealed natural down regulation of *Tcf7* in the two activated Maf and Ikzf2 T_{reg} clusters, relative to the cT_{reg} clusters. Polyposis caused T_{reg} activation and expression of genes associataed with both inflammation and immune suppression by T_{reg}s. Therefore, TCF1 deficient T_{reg}s share functional characteristics with T_{reg}s in polyposis.

Our findings were confirmed by FACS and functional studies. We detected increased expression of activation markers and components of the TGFβ signaling pathway at the protein level. Using *ex vivo* and *in vivo* assay we demonstrated that TCF1 deficient T_{reg}s strongly suppress the proliferation and antigen-specific T-cell cytotoxicity, but were unable to hinder the polarization of CD4^{+} T-cell to the pro-inflammatory T_H17 or T_H1 lineages. TCF1-deficient T_{reg}s increased tumor burden and aggression in mice genetically predisposed to polyposis. These findings demonstrate that TCF1 coordinates Treg activation and independent Treg suppressive activities, in a manner that is relevant to the role of T_{reg}s in cancer. It is noteworthy that T_{reg}s with pro-inflammatory properties are not restricted to the cancer pathology, and are also present in individuals infected with hepatitis A[125] as well as in fungal and bacterial infections, as reviewed in [126, 127]. Thus, the TCF1 fine tuning of T_{reg} functions has physiological relevance.

While TCF1 promotes T_H17 properties in T_{reg}s, we provide evidence that this coincides with increased T-cell suppressive function of T_{reg}s. Enhanced TGFβ signaling together with Wnt signaling is likely to have a central

role in this bimodal change of T_{reg} properties. TGFβ signaling is essential for both thymic and extrathymic generation of T_{reg}s, for maintaining stable expression of Foxp3 [128] (for review see [129]), and for T_{reg} suppression of $CD8^+$ T-cell cytotoxicity[51, 52]. Notably, pharmacologic inhibition of TGFβR1 signaling blocked T_{reg} suppression of CD8 cytotoxicity by TCF1 deficiet T_{reg}s, emphasizing the critical role of TGFβ signaling in this process. TGFβ signaling can also promote T_H17 polarization, for example when combined with IL6 or IL1β [130]. Therefore, TGFβ signaling and upregulation of RORγt, which is a downstream target of IL6 and IL1β, can synergize to reverse the anti-inflammatory properties of TCF1 deficient T_{reg}s. The functional properties of TCF1-deficient T_{reg}s in healthy mice are reminiscent to those of T_{reg}s in cancer patients and mouse models of polyposis/CRC, including elevated expression of RORγt, enhanced Wnt and T_H17 signaling, and tumor promoting function in CRC[131]. Therefore, tumors exploit the β-catenin/TCF1/RORγt axis to its' own advantage, and this pathway is a potential target for immune therapy of CRC.

Our detailed analyses of genes and processes affected by the loss of TCF1 in T_{reg}s elucidate the molecular basis of regulation of T_{reg} functional diversity, and have translational implications. The identified genes and pathways can be targeted to modulate T_{reg} functions and limit disease. We posit that signaling pathways which overlap between down regulation of TCF1 and upregulation of β-catenin may be most relevant to the gain of pro-inflammatory and tumor properties by T_{reg}s. Therefore, we think that our findings could help to both understand fundamental mechanisms of regulation of T_{reg} functions and provide the basis for future translational studies aimed at cancer detection and therapy.

Materials and Methods

Mice

Mouse strains described below were housed and bred at the Mayo Clinic animal facility. *Tcf7*$^{fl/fl}$ (European Mouse Mutant Archive, EMMA)[40] were crossed to *Foxp3*$^{Cre\text{-}YFP}$ mice[41] (designated as *Foxp3*^{Cre} mice) to generate T_{reg} cell-specific *Tcf7* deletion strains. *Foxp3*^{Cre}*Tcf7*$^{fl/fl}$ and control *Foxp3*^{Cre} were crossed to *Apc*$^{\Delta 468}$ [122] and *Il10.*Thy1.1[132] strains to generate *Apc*$^{\Delta 468}$*Foxp3*^{Cre}*Tcf7*$^{fl/fl}$ and *Apc*$^{\Delta 468}$ *Foxp3*^{Cre}, and *Foxp3*^{Cre}*Tcf7*$^{fl/fl}$*Il10.*Thy1.1

and *Foxp3*^{Cre}*Il10.*Thy1.1 mice. Animal experiments were approved by the Animal Ethics Committee of the institutes responsible for housing the mice. Unless otherwise specified, all experimental procedures were performed on 5.5-6-month-old laboratory mice.

Viral infections

Mice were infected with Theiler's encephalomyelitis virus (TMEV) at day 0. For acute viral infection, 2.5-5.0 × 10^5 plaque-forming units (PFU) was used. Virus was prepared in plain DMEM and injected intraperitoneally (i.p.).

***In vivo* cytotoxicity assay**

In vivo CTL assays followed established protocols[52, 133]. Briefly, splenocytes from naive WT CD45.1 background mouse were prepared as single-cell suspensions to 1 × 10^7/ml in Ca/Mg-free Hanks' balanced salt solution (HBSS) (GE Healthcare). The specific target population (half of the cells) was pulsed with 1μM/ml $VP2_{121-130}$ peptide and the negative control target population (half of the cells) was not pulsed with peptide. Cells were incubated for 60 min at 37 °C, then were washed twice in complete media and brought up in Ca/Mg-free HBSS for labeling with carboxyfluorescein succinimidyl ester (CFSE; 79898 BioLegend). Peptide pulsed cells were incubated with 10 μM CFSE ($CFSE^{hi}$) or non-pulsed with 1 μM CFSE ($CFSE^{lo}$) concentrations for 10 min in a 37 °C water bath, and then quenched by addition of complete media. Cells were washed three times, then viable cells counted and mixed in a 1:1 ratio prior to injection into recipient mice. A total of 15 million cells per 200 μl Ca/Mg-free PBS (Lonza) (at room temperature) were transferred into mice on day 7 post TMEV, by *i.v.* injection into the tail. Recipient mice were euthanized 4 h later, and the harvested mesenteric lymph nodes and splenocytes were analyzed by flow cytometry to determine the percentage of $CFSE^{hi}$ and $CFSE^{lo}$ cells. The percentage of $VP2_{121-130}$ -specific cytotoxicity was calculated as follows:

$$\%\ \text{specific lysis} = 1 - \frac{rnaive}{rinfected}\ x\ 100.\ r = \frac{\%\ CFSE^{lo}\ cells}{\%\ CFSE^{hi}\ cells}$$

In some experiments, mice were gavaged twice a day with TGFβR1 inhibitor (LY3200882, Eli Lilly) 105 mg/kg body weight or 1% hydroxyethyl-cellulose (09368; Sigma) as vehicle from the day of infection till day 7 post infection. Then the cytotoxicity was measured as described above.

Dissociation of mesenteric lymph nodes (MLNs) and spleen

A single cell suspension was obtained from MLNs and splenocytes after physical dissociation with a 40 µm mesh (Falcon). Red blood cell lysis on splenocytes was performed using 1 ml of ACK lysis buffer (Lonza) for 1 min on ice and washed in PBS-2% FBS (F8067; Sigma) buffer.

Enzymatic dissociation of small bowel and colon

Tissue was dissociated using the following steps. Fat layers were removed, washed, and opened longitudinally. Tissues were then minced and dissociated in a cocktail solution of 12 mg collagenase IV (LS004188; Worthington), 180 U DNase (D5025; Sigma) and 1.2 mg hyaluronidase (H3506; Sigma) in 20 ml complete media with constant stirring for 25 min at 37 ^{o}C. Single cell suspensions were then filtered, and supernatants were washed in PBS-2% FBS. Tissues were digested twice. A percoll (P1644; Sigma) gradient was then performed to remove platelets and debris by layering the 44 % percoll cell suspension over 67 % percoll and centrifuging at 400 g for 20 min at 4 ^{o}C without brake. The mononuclear cell layer was collected and washed in PBS-2% FBS buffer.

Flow cytometry

Cells were stained with LIVE/DEAD Fixable Blue Stain (L34962; Invitrogen) and antibodies. The fluorochrome-conjugated antibodies were as follows: anti-CD4-PerCP/Cyanine5.5 (RM4-5), anti-CD25-Brilliant Violet 650 (PC61), anti-CD44-Brilliant Violet 785 (IM7), anti-CD278 (ICOS)-PE-Cy7 (C398.4A), anti-CD279 (PD-1)-Brilliant Violet 421 (29F.1A12), anti-CD45.1-PE/Cy7 (A20) (all from BioLegend); anti-CD8a-V500 (53-6.7), anti-CD62L-FITC (MEL-14), anti-CD69-Brilliant Violet 785 (H1.2F3), anti-GITR-PE-Cy7 (DTA-1), anti-CD45.2-APC (clone 104) (all from BD Biosciences). 50 µl of a 1:50 dilution of APC-conjugated D^{b}:$VP2_{121-130}$ tetramer (National Institutes of Health Tetramer Core Facility) was used in a 30-min incubation step in the dark at room temperature. Tgfβ RI-PE (FAB5871P), Rat IgG2A-PE (IC006P), Tgfβ RII-PE (FAB532P) and Goat IgG-PE (IC108P; all from R & D Systems) surface staining were performed according to the manufacturer's instruction. For intracellular staining, surface-stained cells were fixed and permeabilized with the Foxp3/Transcription Factor Staining Buffer Set (00-5523-00; eBiosciences), followed by incubation with fluorochrome-conjugated anti-Foxp3-APC (FJK-

16s; eBioscience); anti-Helios-PerCP/Cyanine5.5 (22F6; BioLegend); anti-RORγT-Brilliant Violet 421 (Q31-378; BD Biosciences); and anti-TCF1/TCF7-Alexa Fluor 647 (C63D9; Cell Signaling) for 2 h or overnight at 4 °C. Cells were then washed twice with wash/perm buffer.

For detection of phosphorylated signaling proteins (S6 and STAT5), lymphocytes were rested in complete medium for 1 h at 37 °C. They were fixed with Phosflow Lyse/ Fix buffer (558049; BD Biosciences), followed by permeabilization with Phosflow Perm buffer III (558050; BD Biosciences) and were stained with antibody to PE-conjugated S6 phosphorylated at Ser235 and Ser236 (D57.2.2E) and rabbit IgG-PE (DA1E; both from Cell Signaling Technology), FITC-conjugated STAT5 phosphorylated at Tyr694 **(**SRBCZX**)** and Mouse IgG1 kappa-FITC (P3.6.2.8.1; both from eBioscience).

For detection of phosphorylated signaling proteins (Smad2/Smad3), lymphocytes were rested in serum free media for 3 h at 37 °C, prior to 15 min stimulation with 10 ng/ml of Tgfβ1 (Peprotech). They were fixed with Phosflow Lyse/ Fix buffer, followed by permeabilization with Phosflow Perm buffer III and were stained with antibody to PE-conjugated Smad2/Smad3 phosphorylated at Ser465/467 and Ser423/425 (D27F4) and rabbit IgG-PE (DA1E; both from Cell Signaling Technology).

All flow cytometry data were acquired on LSRII or LSR Fortessa (BD Biosciences) and analyzed with Flowjo software (Tree Star).

In vivo T_H1 polarization and intracellular IFN-γ staining

Mice were injected *i.p.* with TMEV or carrier as control and euthanized after 7 days. Mesenteric lymph nodes and spleen were collected. Single cells suspension was prepared and stimulated with 50 ng/ml phorbol-12-myristate-13-acetate (PMA, P1585; Sigma) and 0.75 μg/ml ionomycin (13909; Sigma) for 5 h in the presence of 1 μg/ml GolgiStop (555029; BD Biosciences) before intracellular staining. Cells were surface-stained followed by Ifnγ (XMG1.2; eBioscience) intracellular staining.

In vivo T_H17 polarization and intracellular IL17 staining

Mice were injected intraperitoneally three times with CD3-specific antibody (20 μg per mouse; 2C11; BioLegend) or PBS at 0, 48 and 96 h[121]. 100 h after the first injection, the small bowel was enzymatically dispersed,

intraepithelial cells (ILC) and lamina propria (LP) cells were isolated, and re-stimulated with PMA/Ionomycin and 5 h later were stained for intracellular IL-17A (TC11-18H10; BD Biosciences).

***In vitro* T cell polarization assay**

Total CD4+ T cells from spleen of *Foxp3*^{Cre} and *Foxp3*^{Cre}*Tcf7*$^{fl/fl}$ mice were negatively isolated through the use of a mouse CD4$^+$ T Cell Isolation Kit (130-104-454; Miltenyi). 1 × 10^5 CD4$^+$ T cells were seeded with 1 × 10^5 irradiated APC, 0.75 μg/ml anti-CD3 (2C11; BioLegend) and 1 μg/ml anti-CD28 (37.51; BioLegend) in a coated plate. For T_H1 polarization, cells were supplemented with 5 μg/ml of anti-IL-4 (11B11; BD Biosciences), 10 ng/ml of Ifnγ (485-MI-100; R & D Systems), and 10 ng/ml of IL-12 (419-ML; R & D Systems). For T_H17 polarization, cells were treated with 5 μg/ml of anti-IL-4, 5 μg/ml of anti-Ifnγ (XMG1.2; eBioscience), 10 μg/ml of anti-IL-2 (JES6-5H4; Bio Cell), 30 ng/ml of IL-6 (406-ML; R & D Systems) and 1.5 ng/ml of Tgfβ1 (PHG9204; Thermo Fisher). 90 h after activation, cells were re-stimulated with PMA/ionomycin/GolgiStop for 5 h, followed by Ifnγ and IL17A staining.

In other experiments, CD4$^+$CD25$^-$CD62L^{hi}CD44^{lo} naïve T cells were FACS sorted from MACS-pre-purified naïve CD4$^+$ T cells (130-104-453; Miltenyi) isolated from spleen of WT CD45.1 mouse and labeled with 4 μM Cell Trace Violet (C34557; Thermo Fisher). CD25$^+$YFP$^+$ CD45.2 T_{reg}s were FACS sorted from MACS-pre-purified CD4$^+$ T cells (130-104-454; Miltenyi) isolated from spleen of *Foxp3*^{Cre} and *Foxp3*^{Cre}*Tcf7*$^{fl/fl}$ mice. Cells in equal number were stimulated under T_H1 or T_H17 polarized conditions in presence of irradiated splenocytes at 1:1:3 ratio for 90 h. Cells were cultured in RPMI-1640 with L-glutamine (12-702F; Lonza) with 10% FBS, 0.5 mM L-glutamine (25030-081; Life Technologies), 1 mM Sodium pyruvate (Sigma), 100 IU/ml penicillin and 100 mg/ml streptomycin (15140-122; both from Life Technologies), 50 μM/ml β-mercaptoethanol (M3148; Sigma). All cultures were performed in a volume of 200 μl in 96-well U-bottomed plates.

T-cell proliferation suppression assay

CD25$^+$YFP$^+$ CD45.2 T_{reg}s as suppressor cells were FACS sorted from MACS-pre-purified CD4$^+$ T cells (130-104-454; Miltenyi) isolated from spleen of *Foxp3*^{Cre} and *Foxp3*^{Cre}*Tcf7*$^{fl/fl}$ mice. CD4$^+$CD25$^-$CD62L^{hi}CD44^{lo} naïve T cells as responder cells were FACS sorted from MACS-pre-purified naïve CD4$^+$ T cells (130-104-453; Miltenyi)

isolated from spleen of WT CD45.1 mouse. T responder cells were labeled with 2.5 μM CFSE and then cocultured with T_{reg} cells (30×10^3) at a 1:1 ratio with or without allogeneic DC (120×10^3) for 72 h. Allogeneic DC from Balb/c mice was obtained by incubation with MACS microbeads coated with anti-CD11c mAb (130-104-453; Miltenyi Biotech) and irradiated at 3,000 rad. Cells were activated with anti-CD3 (0.5 μg/ml) by coating 96-well round bottom plates for 2 h at 37 °C.

Histology and immune staining

Gut tissues were harvested, opened longitudinally and fixed using 10% formalin for 12–18 h, and routinely paraffin embedded and processed. For immune staining, 5-micron-thick tissue sections were deparaffinized in xylene and rehydrated in ethanol. Following rehydration, slides were immersed in target retrieval solution (S1699; Dako), and heat-induced epitope retrieval was performed in a Decloaking Chamber (Biocare Medical). Following antigen retrieval, tissues were washed with PBS and nonspecific background staining was blocked using dual endogenous enzyme block (S2003; Dako), Fc-block (2.4G2, Antibody Hybridoma Core, Mayo Clinic; kindly provided by Dr Tom Beito), and Background Sniper (BS966L; BioCare Medical). Nonspecific avidin/biotin was blocked when needed (SP-2001; Vector Laboratories). Primary antibodies were diluted in antibody diluent solution (S0809; Dako) and incubated overnight at 4 °C. For β-catenin staining, anti-β-catenin (14/ β-catenin (RUO); BD Biosciences) as primary and Envision + System-HRP-labelled polymer anti-mouse (K4001; Dako) as a secondary antibody was used for 45 min. For Gr1 staining, anti-Gr1 (NIMP-R14; Novus Biologicals) as primary and biotinylated rabbit anti-rat (BA-4001; Vector Laboratories) as secondary antibodies were applied to the sections for 45 min, followed by streptavidin (HRP conjugate, 016-030-084; Jackson Laboratories) for 30 min. Counterstaining was done using Chromogen DAB+Substrate (K3468; Dako) followed by hematoxylin counterstain. A Leica light microscope mounted with a Zeiss Axiocam 503 camera was used for imaging of Immunohistochemistry staining.

mRNA isolation for RNA sequencing

2-4.0 x 10^5 $CD25^+YFP^+$ T_{reg}s were FACS sorted from MACS-pre-purified $CD4^+$ T cells (mouse $CD4^+$ T Cell Isolation Kit, Miltenyi) isolated from MLNs of *Foxp3*^{Cre} and *Foxp3*^{Cre}*Tcf7*$^{fl/fl}$ mice. Total RNA was isolated using

the PicoPure RNA Isolation Kit (Arcturus) following the manufacturer's instructions. Libraries were generated and sequenced by the University of Chicago Genomics Facility.

scRNA sequencing

Whole live cells were washed twice in 1× PBS + 0.04% BSA and immediately submitted to the Core for Single Cell sorting. The cells were first counted and measured for viability using the Vi-Cell XR Cell Viability Analyzer (Beckman-Coulter), as well as a basic hemocytometer with light microscopy. The barcoded Gel Beads were thawed from -80°C and the reverse transcription master mix was prepared according to the manufacturer's instructions for Chromium Single Cell 3' v2 library kit (10x Genomics). Based on the desired number of cells to be captured for each sample, a volume of live cells was mixed with the master mix. The cell suspension/master mix, thawed Gel Beads and partitioning oil were added to a Chromium Single Cell A chip. The filled chip was loaded into the Chromium Controller, where each sample was processed and the individual cells within the sample were captured into uniquely labeled GEMs (Gel Beads-In-Emulsion). The GEMs were collected from the chip and taken to the bench for reverse transcription, GEM dissolution, and cDNA clean-up. Resulting cDNA was a pool of uniquely barcoded molecules. Single cell libraries were created from the cleaned and measured, pooled cDNA. During library construction, standard Illumina sequencing primers and unique i7 Sample indices were added to each cDNA pool. Each sample was uniquely indexed.

All cDNA pools and resulting libraries were measured using Qubit High Sensitivity assays (Thermo Fisher Scientific), Agilent Bioanalyzer High Sensitivity chips (Agilent) and Kapa DNA Quantification reagents (Kapa Biosystems).

Libraries were sequenced at 50,000 fragment reads per cell following Illumina's standard protocol using the Illumina cBot and HiSeq 3000/4000 PE Cluster Kit. The flow cells were sequenced as 100 X 2 paired end reads on an Illumina HiSeq 4000 using HiSeq 3000/4000 sequencing kit and HCS v3.3.52 collection software. Base-calling was performed using Illumina's RTA version 2.7.3.

Single cell RNA-Seq data analysis

The 10X Genomics Cellranger (v2.0.2) mkfastq was applied to demultiplex the Illumina BCL output into FASTQ files. Cellranger count was then applied to each FASTQ file to align reads to mm10 reference genome and generate barcode and UMI counts. We followed the Seurat (v3.2.2) integrated analysis and comparative analysis workflows to do all scRNA-Seq analyses [61]. Genes expressed in < 3 cells and cells with < 200 genes or > 15% mitochondrial genes were excluded for downstream analysis in each dataset. Cell cycle score for each cell was calculated by CellCycleScoring function from Seurat using mouse cell cycle genes. SCTransform function was invoked to normalize the dataset (using default parameters), regress out mitochondrial (percent.MT) and cell cycle (S and G2M) contents and identify variable genes.

The datasets were integrated based on “anchors” identified between datasets (nfeatures = 2000, normalization.method = "SCT") prior to performing linear dimensional reduction by Principal Component Analysis (PCA). The top 25 PCs were included in a Uniform Manifold Approximation and Projection (UMAP) dimensionality reduction. Clusters were identified on a shared nearest neighbor (SNN) graph the top 25 PCs with the Louvain algorithm. Differential gene expression was determined by “findMarkers” function with the default Wilcox Rank Sum test either as one versus rest or as a direct comparison with parameters min.pct = 0.1 and logfc.threshold = 0. For Metascape analysis, the 200 upregulated genes were then determined based on reported adjusted p-values. For GSEA analysis, a pre-ranked gene list was created based on sorted scores defined by $-\log_{10}$(reported p-value)$\times$sign(reported average logfc). The cell annotation was based on the top differentially expressed genes.

Gene list module scores were calculated with Seurat function AddModuleScore [134]. This calculates the average scaled expression levels of each gene list, subtracted by the expression of control feature sets. To compare the single marker expression between cell types, wilcox-test was used.

To calculate the RNA velocity, the loom files were generated from the bam files by Velocyto [104]; The RNA velocity was then calculated using the RunVelocity function in Velocyto.R package. The velocity for each sample was shown by show.velocity.on.embedding.cor function in Velocyto.R package.

Quantification and statistical analysis

Except for deep-sequencing data, statistical significance was calculated with GraphPad Prism software. Error bars in graphs indicate standard error of the mean (SEM) and statistical comparisons were done by unpaired Student's t-test. *p* values of ≤ 0.05 were considered statistically significant.

Acknowledgments

This works was supported by R01 AI 108682 (NIH: FG & KK), RO1 AI 147652 (NIH; FG), and Praespero Innovation Award (Alberta, Caanda; FG & KK). Ms Nicoleta Carapanceanu and Mr. Valentin Carapanceanu are thankfully acknowledged for excellent technical support. Dr. Leesaa Pennell (Biolegend) is gratefully acknowledged for advice with single cell RNA sequencing techniques. Ms. Vernadette Simon (Mayo Clinic, Rochester, MN) is gratefully acknowleged for assistance with single cell RNA sequencing. Dr. Alexandra Vitko Lucs (Eli Lilly) is thankfully acknowledged for providing the TGFβR1 inhibitor LY3200882 and for scientific advice. We thank Dr. Katrina Woolcock (Lifesciences Editors) for professional editing of the manuscript.

Author Contributions

Abu Osman: Performed experiemtns, acquired, analyzed and interpreted data, helped with writing of the manuscript

Kevin Pavelko, Jasmine Quandt, Abdulrahman Saadalla, Mahendra Rathore: Performed experiemtns, acquired and analyzed data.

Bingyu Yan, Ying Li: Performed scRNA analysis and prepared figures, helped with the interpretation of data and writing of the manuscript.

Majid Kazemian, Fotini Gounari, Khashayarsha Khazaie: Analyzed and interpreted data, prepared figures, wrote manuscript.

Khashayarsha Khazaie: Planned, designed, and oversaw experiments.

Conflicting Interests

The authors have no conflicting interests.

Bibliography

Uncategorized References

1. Fontenot, J.D., Gavin, M.A. & Rudensky, A.Y. Foxp3 programs the development and function of CD4+CD25+ regulatory T cells. *Nat Immunol* **4**, 330-336 (2003).

2. Hori, S., Nomura, T. & Sakaguchi, S. Control of regulatory T cell development by the transcription factor Foxp3. *Science* **299**, 1057-1061 (2003).

3. Khattri, R., Cox, T., Yasayko, S.A. & Ramsdell, F. An essential role for Scurfin in CD4+CD25+ T regulatory cells. *Nat Immunol* **4**, 337-342 (2003).

4. Benoist, C. & Mathis, D. Treg cells, life history, and diversity. *Cold Spring Harb Perspect Biol* **4**, a007021 (2012).

5. Lochner, M. *et al.* In vivo equilibrium of proinflammatory IL-17+ and regulatory IL-10+ Foxp3+ RORgamma t+ T cells. *J Exp Med* **205**, 1381-1393 (2008).

6. Ohnmacht, C. *et al.* MUCOSAL IMMUNOLOGY. The microbiota regulates type 2 immunity through RORgammat(+) T cells. *Science* **349**, 989-993 (2015).

7. Sefik, E. *et al.* MUCOSAL IMMUNOLOGY. Individual intestinal symbionts induce a distinct population of RORgamma(+) regulatory T cells. *Science* **349**, 993-997 (2015).

8. Wohlfert, E.A. *et al.* GATA3 controls Foxp3(+) regulatory T cell fate during inflammation in mice. *J Clin Invest* **121**, 4503-4515 (2011).

9. Wang, Y., Su, M.A. & Wan, Y.Y. An essential role of the transcription factor GATA-3 for the function of regulatory T cells. *Immunity* **35**, 337-348 (2011).

10. Koch, M.A. *et al.* The transcription factor T-bet controls regulatory T cell homeostasis and function during type 1 inflammation. *Nat Immunol* **10**, 595-602 (2009).

11. Levine, A.G. *et al.* Corrigendum: Stability and function of regulatory T cells expressing the transcription factor T-bet. *Nature* **550**, 142 (2017).

12. Levine, A.G. *et al.* Stability and function of regulatory T cells expressing the transcription factor T-bet. *Nature* **546**, 421-425 (2017).

13. Wheaton, J.D., Yeh, C.H. & Ciofani, M. Cutting Edge: c-Maf Is Required for Regulatory T Cells To Adopt RORgammat(+) and Follicular Phenotypes. *J Immunol* **199**, 3931-3936 (2017).

14. Xu, M. *et al.* c-MAF-dependent regulatory T cells mediate immunological tolerance to a gut pathobiont. *Nature* **554**, 373-377 (2018).

15. Neumann, C. *et al.* c-Maf-dependent Treg cell control of intestinal TH17 cells and IgA establishes host-microbiota homeostasis. *Nat Immunol* **20**, 471-481 (2019).

16. Schiering, C. *et al.* The alarmin IL-33 promotes regulatory T-cell function in the intestine. *Nature* **513**, 564-568 (2014).

17. He, Z. *et al.* Epithelial-derived IL-33 promotes intestinal tumorigenesis in Apc (Min/+) mice. *Scientific reports* **7**, 5520 (2017).

18. Peine, M., Marek, R.M. & Lohning, M. IL-33 in T Cell Differentiation, Function, and Immune Homeostasis. *Trends Immunol* **37**, 321-333 (2016).

19. Molofsky, A.B., Savage, A.K. & Locksley, R.M. Interleukin-33 in Tissue Homeostasis, Injury, and Inflammation. *Immunity* **42**, 1005-1019 (2015).

20. Pastille, E. *et al.* The IL-33/ST2 pathway shapes the regulatory T cell phenotype to promote intestinal cancer. *Mucosal Immunol* **12**, 990-1003 (2019).

21. Hatzioannou, A. *et al.* An intrinsic role of IL-33 in Treg cell-mediated tumor immunoevasion. *Nat Immunol* **21**, 75-85 (2020).

22. Zhou, Y., Ji, Y., Wang, H., Zhang, H. & Zhou, H. IL-33 Promotes the Development of Colorectal Cancer Through Inducing Tumor-Infiltrating ST2L(+) Regulatory T Cells in Mice. *Technol Cancer Res Treat* **17**, 1533033818780091 (2018).

23. Blatner, N.R. *et al.* Expression of RORgammat marks a pathogenic regulatory T cell subset in human colon cancer. *Sci Transl Med* **4**, 164ra159 (2012).

24. Yissachar, N. *et al.* An Intestinal Organ Culture System Uncovers a Role for the Nervous System in Microbe-Immune Crosstalk. *Cell* **168**, 1135-1148 e1112 (2017).

25. Pratama, A., Schnell, A., Mathis, D. & Benoist, C. Developmental and cellular age direct conversion of CD4(+) T cells into RORgamma(+) or Helios(+) colon Treg cells. *J Exp Med* (2019).

26. Miragaia, R.J. *et al.* Single-Cell Transcriptomics of Regulatory T Cells Reveals Trajectories of Tissue Adaptation. *Immunity* **50**, 493-504 e497 (2019).

27. Osorio, F. *et al.* DC activated via dectin-1 convert Treg into IL-17 producers. *Eur J Immunol* **38**, 3274-3281 (2008).

28. Ayyoub, M. *et al.* Human memory FOXP3+ Tregs secrete IL-17 ex vivo and constitutively express the T(H)17 lineage-specific transcription factor RORgamma t. *Proc Natl Acad Sci U S A* **106**, 8635-8640 (2009).

29. Blatner, N.R. *et al.* In colorectal cancer mast cells contribute to systemic regulatory T-cell dysfunction. *Proc Natl Acad Sci U S A* **107**, 6430-6435 (2010).

30. Keerthivasan, S. *et al.* beta-Catenin promotes colitis and colon cancer through imprinting of proinflammatory properties in T cells. *Sci Transl Med* **6**, 225ra228 (2014).

31. Gounaris, E. *et al.* T-regulatory cells shift from a protective anti-inflammatory to a cancer-promoting proinflammatory phenotype in polyposis. *Cancer Res* **69**, 5490-5497 (2009).

32. Sumida, T. *et al.* Activated beta-catenin in Foxp3(+) regulatory T cells links inflammatory environments to autoimmunity. *Nat Immunol* **19**, 1391-1402 (2018).

33. Verbeek, S. *et al.* An HMG-box-containing T-cell factor required for thymocyte differentiation. *Nature* **374**, 70-74 (1995).

34. Mosimann, C., Hausmann, G. & Basler, K. Beta-catenin hits chromatin: regulation of Wnt target gene activation. *Nature reviews. Molecular cell biology* **10**, 276-286 (2009).

35. van Loosdregt, J. *et al.* Canonical wnt signaling negatively modulates regulatory T cell function. *Immunity* **39**, 298-310 (2013).

36. Xing, S. *et al.* Tcf1 and Lef1 are required for the immunosuppressive function of regulatory T cells. *J Exp Med* **216**, 847-866 (2019).

37. Mielke, L.A. *et al.* TCF-1 limits the formation of Tc17 cells via repression of the MAF-RORgammat axis. *J Exp Med* **216**, 1682-1699 (2019).

38. Barra, M.M., Richards, D.M., Hofer, A.C., Delacher, M. & Feuerer, M. Premature expression of Foxp3 in double-negative thymocytes. *PLoS One* **10**, e0127038 (2015).

39. Barra, M.M. *et al.* Transcription Factor 7 Limits Regulatory T Cell Generation in the Thymus. *J Immunol* **195**, 3058-3070 (2015).

40. Emmanuel, A.O. *et al.* TCF-1 and HEB cooperate to establish the epigenetic and transcription profiles of CD4(+)CD8(+) thymocytes. *Nat Immunol* **19**, 1366-1378 (2018).

41. Rubtsov, Y.P. *et al.* Regulatory T cell-derived interleukin-10 limits inflammation at environmental interfaces. *Immunity* **28**, 546-558 (2008).

42. Zemmour, D. *et al.* Single-cell gene expression reveals a landscape of regulatory T cell phenotypes shaped by the TCR. *Nat Immunol* **19**, 291-301 (2018).

43. Sakaguchi, S., Sakaguchi, N., Asano, M., Itoh, M. & Toda, M. Immunologic self-tolerance maintained by activated T cells expressing IL-2 receptor alpha-chains (CD25). Breakdown of a single mechanism of self-tolerance causes various autoimmune diseases. *J Immunol* **155**, 1151-1164 (1995).

44. Gavin, M.A. *et al.* Foxp3-dependent programme of regulatory T-cell differentiation. *Nature* **445**, 771-775 (2007).

45. Samstein, R.M. *et al.* Foxp3 exploits a pre-existent enhancer landscape for regulatory T cell lineage specification. *Cell* **151**, 153-166 (2012).

46. Luo, C.T. & Li, M.O. Foxo transcription factors in T cell biology and tumor immunity. *Semin Cancer Biol* **50**, 13-20 (2018).

47. Kerdiles, Y.M. *et al.* Foxo transcription factors control regulatory T cell development and function. *Immunity* **33**, 890-904 (2010).

48. Hsu, P. *et al.* IL-10 Potentiates Differentiation of Human Induced Regulatory T Cells via STAT3 and Foxo1. *J Immunol* **195**, 3665-3674 (2015).

49. Luo, C.T., Liao, W., Dadi, S., Toure, A. & Li, M.O. Graded Foxo1 activity in Treg cells differentiates tumour immunity from spontaneous autoimmunity. *Nature* **529**, 532-536 (2016).

50. Marie, J.C., Liggitt, D. & Rudensky, A.Y. Cellular mechanisms of fatal early-onset autoimmunity in mice with the T cell-specific targeting of transforming growth factor-beta receptor. *Immunity* **25**, 441-454 (2006).

51. Fahlen, L. *et al.* T cells that cannot respond to TGF-beta escape control by CD4(+)CD25(+) regulatory T cells. *J Exp Med* **201**, 737-746 (2005).

52. Chen, M.L. *et al.* Regulatory T cells suppress tumor-specific CD8 T cell cytotoxicity through TGF-beta signals in vivo. *Proc Natl Acad Sci U S A* **102**, 419-424 (2005).

53. Yang, B.H. *et al.* TCF1 and LEF1 Control Treg Competitive Survival and Tfr Development to Prevent Autoimmune Diseases. *Cell Rep* **27**, 3629-3645 e3626 (2019).

54. Mucida, D. *et al.* Reciprocal TH17 and regulatory T cell differentiation mediated by retinoic acid. *Science* **317**, 256-260 (2007).

55. Mucida, D. *et al.* Retinoic acid can directly promote TGF-beta-mediated Foxp3(+) Treg cell conversion of naive T cells. *Immunity* **30**, 471-472; author reply 472-473 (2009).

56. Wielenga, V.J. *et al.* Expression of CD44 in Apc and Tcf mutant mice implies regulation by the WNT pathway. *Am J Pathol* **154**, 515-523. (1999).

57. van de Wetering, M. *et al.* The beta-catenin/TCF-4 complex imposes a crypt progenitor phenotype on colorectal cancer cells. *Cell* **111**, 241-250 (2002).

58. Zeng, H. *et al.* mTORC1 couples immune signals and metabolic programming to establish T(reg)-cell function. *Nature* **499**, 485-490 (2013).

59. Procaccini, C. *et al.* An oscillatory switch in mTOR kinase activity sets regulatory T cell responsiveness. *Immunity* **33**, 929-941 (2010).

60. Chapman, N.M. & Chi, H. mTOR Links Environmental Signals to T Cell Fate Decisions. *Front Immunol* **5**, 686 (2014).

61. Butler, A., Hoffman, P., Smibert, P., Papalexi, E. & Satija, R. Integrating single-cell transcriptomic data across different conditions, technologies, and species. *Nat Biotechnol* **36**, 411-420 (2018).

62. Sebastian, M. *et al.* Helios Controls a Limited Subset of Regulatory T Cell Functions. *J Immunol* **196**, 144-155 (2016).

63. Thornton, A.M. *et al.* Expression of Helios, an Ikaros transcription factor family member, differentiates thymic-derived from peripherally induced Foxp3+ T regulatory cells. *J Immunol* **184**, 3433-3441 (2010).

64. Morita, H. *et al.* An Interleukin-33-Mast Cell-Interleukin-2 Axis Suppresses Papain-Induced Allergic Inflammation by Promoting Regulatory T Cell Numbers. *Immunity* **43**, 175-186 (2015).

65. Miyazaki, M. *et al.* Id2 and Id3 maintain the regulatory T cell pool to suppress inflammatory disease. *Nat Immunol* **15**, 767-776 (2014).

66. Fazilleau, N. & Aloulou, M. Several Follicular Regulatory T Cell Subsets With Distinct Phenotype and Function Emerge During Germinal Center Reactions. *Front Immunol* **9**, 1792 (2018).

67. Bernhagen, J. *et al.* MIF is a noncognate ligand of CXC chemokine receptors in inflammatory and atherogenic cell recruitment. *Nat Med* **13**, 587-596 (2007).

68. Rajasekaran, D. *et al.* Macrophage Migration Inhibitory Factor-CXCR4 Receptor Interactions: EVIDENCE FOR PARTIAL ALLOSTERIC AGONISM IN COMPARISON WITH CXCL12 CHEMOKINE. *J Biol Chem* **291**, 15881-15895 (2016).

69. Alibashe-Ahmed, M. *et al.* Macrophage migration inhibitory factor regulates TLR4 expression and modulates TCR/CD3-mediated activation in CD4+ T lymphocytes. *Scientific reports* **9**, 9380 (2019).

70. Odegard , J.M. *et al.* ICOS-dependent extrafollicular helper T cells elicit IgG production via IL-21 in systemic autoimmunity. *Journal of Experimental Medicine* **205**, 2873-2886 (2008).

71. Odegard, J.M. *et al.* ICOS-dependent extrafollicular helper T cells elicit IgG production via IL-21 in systemic autoimmunity. *J Exp Med* **205**, 2873-2886 (2008).

72. Hargreaves, D.C. *et al.* A Coordinated Change in Chemokine Responsiveness Guides Plasma Cell Movements. *Journal of Experimental Medicine* **194**, 45-56 (2001).

73. Allen, C.D. *et al.* Germinal center dark and light zone organization is mediated by CXCR4 and CXCR5. *Nat Immunol* **5**, 943-952 (2004).

74. Gore, Y. *et al.* Macrophage migration inhibitory factor induces B cell survival by activation of a CD74-CD44 receptor complex. *J Biol Chem* **283**, 2784-2792 (2008).

75. Radomir, L. *et al.* T Cells Regulate Peripheral Naive Mature B Cell Survival by Cell-Cell Contact Mediated through SLAMF6 and SAP. *J Immunol* **199**, 2745-2757 (2017).

76. Kawamoto, S. *et al.* Foxp3(+) T cells regulate immunoglobulin a selection and facilitate diversification of bacterial species responsible for immune homeostasis. *Immunity* **41**, 152-165 (2014).

77. Bucala, R. & Shachar, I. The integral role of CD74 in antigen presentation, MIF signal transduction, and B cell survival and homeostasis. *Mini Rev Med Chem* **14**, 1132-1138 (2014).

78. Zhou, Y. *et al.* Metascape provides a biologist-oriented resource for the analysis of systems-level datasets. *Nat Commun* **10**, 1523 (2019).

79. Takada, K. *et al.* Kruppel-like factor 2 is required for trafficking but not quiescence in postactivated T cells. *J Immunol* **186**, 775-783 (2011).

80. Weinreich, M.A., Jameson, S.C. & Hogquist, K.A. Postselection thymocyte maturation and emigration are independent of IL-7 and ERK5. *J Immunol* **186**, 1343-1347 (2011).

81. Allende, M.L., Dreier, J.L., Mandala, S. & Proia, R.L. Expression of the sphingosine 1-phosphate receptor, S1P1, on T-cells controls thymic emigration. *J Biol Chem* **279**, 15396-15401 (2004).

82. Drennan, M.B., Elewaut, D. & Hogquist, K.A. Thymic emigration: Sphingosine-1-phosphate receptor-1-dependent models and beyond. *European Journal of Immunology* **39**, 925-930 (2009).

83. James, K.D., Jenkinson, W.E. & Anderson, G. T-cell egress from the thymus: Should I stay or should I go? *Journal of leukocyte biology* **104**, 275-284 (2018).

84. McFarland, R.D., Douek, D.C., Koup, R.A. & Picker, L.J. Identification of a human recent thymic emigrant phenotype. *Proceedings of the National Academy of Sciences* **97**, 4215-4220 (2000).

85. Teng, F. *et al.* The molecular signature underlying the thymic migration and maturation of TCRalphabeta+ CD4+ CD8 thymocytes. *PLoS One* **6**, e25567 (2011).

86. Pabbisetty, S.K. *et al.* Peripheral tolerance can be modified by altering KLF2-regulated Treg migration. *Proc Natl Acad Sci U S A* **113**, E4662-4670 (2016).

87. Nakanishi, Y. *et al.* Regulatory T cells with superior immunosuppressive capacity emigrate from the inflamed colon to draining lymph nodes. *Mucosal Immunol* **11**, 437-448 (2018).

88. Miyagawa, I. *et al.* Induction of Regulatory T Cells and Its Regulation with Insulin-like Growth Factor/Insulin-like Growth Factor Binding Protein-4 by Human Mesenchymal Stem Cells. *J Immunol* **199**, 1616-1625 (2017).

89. Hankinson, O. Role of coactivators in transcriptional activation by the aryl hydrocarbon receptor. *Arch Biochem Biophys* **433**, 379-386 (2005).

90. Beischlag, T.V. *et al.* Recruitment of the NCoA/SRC-1/p160 family of transcriptional coactivators by the aryl hydrocarbon receptor/aryl hydrocarbon receptor nuclear translocator complex. *Mol Cell Biol* **22**, 4319-4333 (2002).

91. Wagner, M. *et al.* NCOA3 is a selective co-activator of estrogen receptor α-mediated transactivation of PLAC1 in MCF-7 breast cancer cells. *BMC Cancer* **13**, 570 (2013).

92. Balderhaar, H.J. *et al.* The CORVET complex promotes tethering and fusion of Rab5/Vps21-positive membranes. *Proc Natl Acad Sci U S A* **110**, 3823-3828 (2013).

93. Balderhaar, H.J. & Ungermann, C. CORVET and HOPS tethering complexes - coordinators of endosome and lysosome fusion. *J Cell Sci* **126**, 1307-1316 (2013).

94. Kalekar, L.A. *et al.* CD4(+) T cell anergy prevents autoimmunity and generates regulatory T cell precursors. *Nat Immunol* **17**, 304-314 (2016).

95. Soto, R. *et al.* Microbiota promotes systemic T-cell survival through suppression of an apoptotic factor. *Proc Natl Acad Sci U S A* **114**, 5497-5502 (2017).

96. Weis, A.M., Soto, R. & Round, J.L. Commensal regulation of T cell survival through Erdr1. *Gut Microbes* **9**, 458-464 (2018).

97. Brenu, E.W. *et al.* Heat shock proteins and regulatory T cells. *Autoimmune Dis* **2013**, 813256 (2013).

98. Kolinski, T., Marek-Trzonkowska, N., Trzonkowski, P. & Siebert, J. Heat shock proteins (HSPs) in the homeostasis of regulatory T cells (Tregs). *Cent Eur J Immunol* **41**, 317-323 (2016).

99. Miao, T. *et al.* Early growth response gene-2 controls IL-17 expression and Th17 differentiation by negatively regulating Batf. *J Immunol* **190**, 58-65 (2013).

100. Wang, C. *et al.* BATF is required for normal expression of gut-homing receptors by T helper cells in response to retinoic acid. *J Exp Med* **210**, 475-489 (2013).

101. Joller, N. *et al.* Treg cells expressing the coinhibitory molecule TIGIT selectively inhibit proinflammatory Th1 and Th17 cell responses. *Immunity* **40**, 569-581 (2014).

102. Lee, Y. *et al.* Induction and molecular signature of pathogenic TH17 cells. *Nat Immunol* **13**, 991-999 (2012).

103. Yosef, N. *et al.* Dynamic regulatory network controlling TH17 cell differentiation. *Nature* **496**, 461-468 (2013).

104. La Manno, G. *et al.* RNA velocity of single cells. *Nature* **560**, 494-498 (2018).

105. Song, X. *et al.* Microbial bile acid metabolites modulate gut RORgamma(+) regulatory T cell homeostasis. *Nature* **577**, 410-415 (2020).

106. Roychoudhuri, R. *et al.* BACH2 regulates CD8(+) T cell differentiation by controlling access of AP-1 factors to enhancers. *Nat Immunol* **17**, 851-860 (2016).

107. Meixner, A., Karreth, F., Kenner, L. & Wagner, E.F. JunD regulates lymphocyte proliferation and T helper cell cytokine expression. *Embo j* **23**, 1325-1335 (2004).

108. Chen, Z. *et al.* Selective regulatory function of Socs3 in the formation of IL-17-secreting T cells. *Proc Natl Acad Sci U S A* **103**, 8137-8142 (2006).

109. Workman, C.J. & Vignali, D.A. The CD4-related molecule, LAG-3 (CD223), regulates the expansion of activated T cells. *Eur J Immunol* **33**, 970-979 (2003).

110. Wang, J. *et al.* Fibrinogen-like Protein 1 Is a Major Immune Inhibitory Ligand of LAG-3. *Cell* **176**, 334-347 e312 (2019).

111. Huang, C.T. *et al.* Role of LAG-3 in regulatory T cells. *Immunity* **21**, 503-513 (2004).

112. Woo, S.R. *et al.* Immune inhibitory molecules LAG-3 and PD-1 synergistically regulate T-cell function to promote tumoral immune escape. *Cancer Res* **72**, 917-927 (2012).

113. Mempel, T.R. *et al.* Regulatory T cells reversibly suppress cytotoxic T cell function independent of effector differentiation. *Immunity* **25**, 129-141 (2006).

114. Pavelko, K.D. *et al.* Theiler's murine encephalomyelitis virus as a vaccine candidate for immunotherapy. *PLoS One* **6**, e20217 (2011).

115. Pavelko, K.D. *et al.* The epitope integration site for vaccine antigens determines virus control while maintaining efficacy in an engineered cancer vaccine. *Mol Ther* **21**, 1087-1095 (2013).

116. Szabo, S.J., Dighe, A.S., Gubler, U. & Murphy, K.M. Regulation of the interleukin (IL)-12R beta 2 subunit expression in developing T helper 1 (Th1) and Th2 cells. *J Exp Med* **185**, 817-824 (1997).

117. Glimcher, L.H. & Murphy, K.M. Lineage commitment in the immune system: the T helper lymphocyte grows up. *Genes Dev* **14**, 1693-1711 (2000).

118. Szabo, S.J. *et al.* A novel transcription factor, T-bet, directs Th1 lineage commitment. *Cell* **100**, 655-669 (2000).

119. Aggarwal, S., Ghilardi, N., Xie, M.H., de Sauvage, F.J. & Gurney, A.L. Interleukin-23 promotes a distinct CD4 T cell activation state characterized by the production of interleukin-17. *J Biol Chem* **278**, 1910-1914 (2003).

120. Bettelli, E., Korn, T. & Kuchroo, V.K. Th17: the third member of the effector T cell trilogy. *Curr Opin Immunol* **19**, 652-657 (2007).

121. Esplugues, E. *et al.* Control of TH17 cells occurs in the small intestine. *Nature* **475**, 514-518 (2011).

122. Gounaris, E. *et al.* Live imaging of cysteine-cathepsin activity reveals dynamics of focal inflammation, angiogenesis, and polyp growth. *PLoS One* **3**, e2916 (2008).

123. Bos, P.D. & Rudensky, A.Y. Treg cells in cancer: a case of multiple personality disorder. *Sci Transl Med* **4**, 164fs144 (2012).

124. Zhang, J. *et al.* TCF-1 Inhibits IL-17 Gene Expression To Restrain Th17 Immunity in a Stage-Specific Manner. *J Immunol* **200**, 3397-3406 (2018).

125. Choi, Y.S. *et al.* Tumor Necrosis Factor-producing T-regulatory Cells Are Associated With Severe Liver Injury in Patients With Acute Hepatitis A. *Gastroenterology* **154**, 1047-1060 (2018).

126. Chen, X. & Oppenheim, J.J. Th17 cells and Tregs: unlikely allies. *J Leukoc Biol* **95**, 723-731 (2014).

127. Whibley, N. & Gaffen, S.L. Brothers in arms: Th17 and Treg responses in Candida albicans immunity. *PLoS Pathog* **10**, e1004456 (2014).

128. Freudenberg, K. *et al.* Critical Role of TGF-beta and IL-2 Receptor Signaling in Foxp3 Induction by an Inhibitor of DNA Methylation. *Front Immunol* **9**, 125 (2018).

129. Tran, D.Q. TGF-beta: the sword, the wand, and the shield of FOXP3(+) regulatory T cells. *J Mol Cell Biol* **4**, 29-37 (2012).

130. Bettelli, E. *et al.* Reciprocal developmental pathways for the generation of pathogenic effector TH17 and regulatory T cells. *Nature* **441**, 235-238 (2006).

131. Blatner, N.R., Gounari, F. & Khazaie, K. The two faces of regulatory T cells in cancer. *Oncoimmunology* **2**, e23852 (2013).

132. Maynard, C.L. *et al.* Regulatory T cells expressing interleukin 10 develop from Foxp3+ and Foxp3- precursor cells in the absence of interleukin 10. *Nat Immunol* **8**, 931-941 (2007).

133. Pavelko, K.D., Bell, M.P., Harrington, S.M. & Dong, H. B7-H1 Influences the Accumulation of Virus-Specific Tissue Resident Memory T Cells in the Central Nervous System. *Front Immunol* **8**, 1532 (2017).

134. Tirosh, I. *et al.* Dissecting the multicellular ecosystem of metastatic melanoma by single-cell RNA-seq. *Science* **352**, 189-196 (2016).

Figure Legends

Figure 1: TCF1 deficiency selectively reprograms T_{reg}s without compromising their core signature. (**a**) Scatter plot comparing the expression of genes in TCF1-sufficient (*Foxp3*^{Cre}) and TCF1-deficient (*Foxp3*^{Cre} *Tcf7*$^{fl/fl}$) T_{reg}s. Reads Per Kilobase of transcript, per Million mapped reads (RPKM) expression values are average of three biological replicates. Significantly up- or downregulated genes (fold change >1.5 and FDR < 0.001) are shown in red or blue with exact numbers shown at the top or bottom corner, respectively. (**b**) Significantly enriched Kegg pathways by gene set enrichment analysis (GSEA) induced in transcriptomes of Tcf1-deficient versus sufficient T_{reg}s. Normalized enrichment scores of all enriched Kegg pathways (FDR< 25%) are shown. Select pathways are highlighted. See TableS1 for the full list. (**c**) The expression of all leading-edge genes from four indicated pathways.

Figure 2: Cumulative data from FACS analysis shows activation and expansion of T_{reg}s and T_{eff} cells in TCF1-deficient mice. T_{reg}s and CD4$^+$ T_{eff} cells from 5.5-month-old *Foxp3*^{Cre} *Tcf7*$^{fl/fl}$ mice and control *Foxp3*^{Cre} mice were analyzed by FACS. **(a)** Frequency of CD4$^+$Foxp3$^+$ T_{reg}s expressing CD69, ICOS, PD-1, and CD44 and CD62L, in MLN and spleen. **(b)** T_{reg} frequency and numbers and expression of CD25 in the MLN and spleen. **(c)** Frequency of conventional CD4$^+$ T-cells expressing CD69, PD-1, ICOS, and CD44 and CD62L, in MLN and spleen. **(d)** The frequency of HELIOS$^-$ or HELIOS$^+$FOXP3$^+$RORγT$^+$ T_{reg}s, in the spleen, MLN, small bowel, and colon. **(e)** Representative FACS histograms normalized to mode (left) and bar diagrams of cumulative data for expression of TGFβR1, TGFβR2, pSMAD2/3, pS6, and pSTAT5 by T_{reg}s. For the cumulative data, each symbol represents a value from an individual mouse. Data are means ± SEM unpaired Student's t test.
* $p < 0.05$; ** $p < 0.01$; *** $p < 0.001$.

Figure 3: Single cell transcriptomics delineate distinct T_{reg} subpopulations in the mesenteric lymph nodes. (**a**) Integrated UMAP showing 10 major cell types in isolated T_{reg}s from mice used in this study. (**b**) Expression of cell-defining features across all cell types. (**c**) mRNA expression of select indicated genes projected on the UMAP. (**d**) Significantly enriched pathways by Metascape based on top 200 genes upregulated in indicated cell type compared to all other cell types. See TableS2 for the full list. (**e**) 20 most significantly

enriched pathways by Metascape based on genes upregulated in Klf2^{-} or Klf2^{++} cell types compared directly to Klf2^{++} or Klf2^{-} cell types, respectively.

Figure 4: TCF1-deficient and sufficient T_{reg}s show distinct effector functions. (**a**) UMAP projection (left) and fraction of cells in each cell type (stackbars; right panel) for TCF1-sufficient (*Foxp3*^{Cre}) and TCF1-deficient (*Foxp3*^{Cre} *Tcf7*$^{fl/fl}$) T_{reg}s. Data are from two replicates. (**b**) Expression changes of the most differentially expressed genes between Tcf1-deficient and sufficient T_{reg}s. See TableS3 for the full list. The fold change in expression intensities is color-coded. The fold change in percent of cells expressing the indicated gene in each cell type is proportional to the circle size. (**c**) Expression of *Maf* (top panel) and *Ccr9* (bottom panel) projected on the UMAP. (**d**) GSEA analysis for the indicated gene lists comparing transcriptomes of Tcf1-sufficient and TCF1-deficient cells across all cell types. Normalized enrichment scores (NES) are color coded. log10 (FDR) values are proportional to the circle size. FDR>15% are masked with gray color. (**e**) Representative GSEA plots from "**d"** comparing TCF1-sufficient and TCF1-deficient Klf2^{-} cells for Stubbington T_H17 and MAF downregulated genes. (**f**) The UMAP projection of module scores for Kegg IL17 signalling pathway and related GSEA. (**g**) map showing observed (cells on the UMAP) and extrapolated future state of cells (overlaid arrows) based on RNA velocity for TCF1-sufficient (*Foxp3*^{Cre}) and TCF1-deficient (*Foxp3*^{Cre} *Tcf7*$^{fl/fl}$) T_{reg}s.

Figure 5: TCF1-deficient T_{reg}s suppress viral antigen specific CD8^{+} T-cell cytotoxicity and T-cell proliferation.

Foxp3^{Cre}*Tcf7*$^{fl/fl}$ and control *Foxp3*^{Cre} mice at 7-8 weeks of age (n = 6-9 per group) were compared for their anti-viral T-cell response. **(a)** Schematic presentation of the *in vivo* kill assay. Mice were gavaged with vehicle or with the Tgfβrl small molecule inhibitor (LY3200882) twice daily starting from the day of viral infection. Specific *in vivo* kill of the $VP2_{121-130}$ pulsed cells was measured by FACS four days after transfer, based on the ratios of the two input cells after correction for cell death in adoptively transferred naïve mice. **(b)** Cumulative data quantified from specific lysis in spleen and MLN. **(c)** Representative FACS histograms of the same assay. **(d)** Tetramer analysis of $VP2_{121-130}$-specific CD8^{+} T-cells of the same assay. **(e)** Schematic presentation of CD4^{+} T-cell proliferation inhibition assay. T cells were purified from the spleen of C57B/6 mice, and T_{reg}s from *Foxp3*^{Cre}*Tcf7*$^{fl/fl}$ mice and control *Foxp3*^{Cre} mice at 5.5 months of age. FACS sorted CD4^{+}CD25^{-} cells were

labelled with CFSE and incubated alone or with irradiated Balb/c DC, with or without equal numbers of T_{reg}s. Dilution of CFSE by CD4 gated cells was measure after 3 days. **(f)** Representative FACS histograms of the same assay. **(g)** Cumulative data of percent of proliferating cells. Each symbol represents a value from an individual mouse. Data are means ± SEM (n = 4-8 per group). **** p < 0.0001, *** p =0.007 or 0.004 as indicated, * p =0.016 or <0.05 as indicated, Student's t test.

Figure 6: TCF1-deficient T_{reg}s fail to suppress T_H1 or T_H17 polarization of $CD4^+$ T_{conv} cells.

Foxp3^{Cre}*Tcf7*$^{fl/f}$ mice and control *Foxp3*^{Cre} mice at 5.5 months of age (n = 5-8 per group) were used as source of T_{reg}s for *in vitro* inhibition of T-helper cells polarization assays, or were used for *in vivo* assays. **(a)** Schematic presentation of *in vitro* T_H1 polarization assay using spleen-derived $CD4^+$ T-cells. **(b)** Total spleen $CD4^+$ cells were magnetically purified from the indicated mice, *in vitro* stimulated for T_H17 polarization for four days and stained for intracellular Ifnγ. Representative FACS contour-plots (left) and cumulative histogram plots (right; n=5) are shown. **(c)** FACS purified $CD62L^+CD44^-CD25^-CD45.1^+CD4^+$ splenocytes were labelled with Cell Trace Violet, mixed 1:1 with $YFP^+CD45.2^+CD4^+CD25^+$ cells, and assayed for T_H1 polarization as described. **(d)** Schematic presentation of *in vitro* T_H17 polarizing assay using spleen-derived $CD4^+$ T-cells. **(e)** $CD4^+$ T-cells were purified as in "b" and after T_H17 polarization were stained for intracellular IL17. **(f)** $CD4^+$ T-cells and T_{reg}s were purified and mixed as in "c" and after T_H17 polarization were stained for intracellular IL17. **(g)** Schematic presentation of induction of *in vivo* T_H1 response to TMEV, and FACS assay. **(h)** Representative FACS contour-plots and cumulative histogram plots showing the extent of T_H1 polarization of $CD4^+$ T-cells as measured by expression of IFNγ. **(i)** The same for $CD8^+$ T-cells. **(j)** Schematic presentation of induction of *in vivo* T_H17 response, and FACS assay. **(k)** Representative FACS contour-plots and cumulative histogram plots showing the extent of T_H17 polarization, measured by staining $CD4^+$ T-cells for intracellular IL17. Each symbol in the cumulative data represents the value from an individual mouse. Data are means ± SEM (n = 5-8 per group). Statistical significance was determined by unpaired Student's t-test. * $p < 0.05$; ** $p < 0.01$; *** $p< 0.001$, **** $p< 0.0001$.

Figure 7. TCF1-deficient T_{reg}s promote inflammation and tumor growth in polyposis-prone Apc$^{\Delta 468}$ mice.

Apc$^{\Delta 468}$*Foxp3*^{Cre}*Tcf7*$^{fl/fl}$ mice and control *Apc*$^{\Delta 468}$*Foxp3*^{Cre} mice were euthanized at 5.5 months of age. Polyp/tumor numbers were counted in the excised gut under a dissection microscope. Tumor aggression was evaluated by staining fixed tissues for β-catenin and counting lesions with extensive staining reaching the border of submucosa. **(a)** Polyp count in the colon, **(b)** polyp count in the small bowel, **(c)** number of invasive lesions in the colon, **(d)** number of invasive lesions in the small bowel. Each symbol represents a value from an individual mouse. Tcf1-sufficient and deficient mice are represented by black and red symbols, respectively. **(e)** Representative immunohistochemistry stains of *Apc*$^{\Delta 468}$*Foxp3*^{Cre}*Tcf7*$^{fl/fl}$ mouse colon and small bowel for nuclear β-catenin. **(f)** The same for *Apc*$^{\Delta 468}$*Foxp3*^{Cre}*Tcf7*$^{fl/fl}$ mouse. **(g)** Quantification of Gr1 stained cells in colon polyps and distant healthy tissue. **(h)** The same in the small bowel. **(i)** Representative immunohistochemistry stains of mouse colon for Gr1. **(j)** The same for small bowel. Each symbol represents counts in one field of vision (FOV) at 200x, from a total of 4 mice per group. Statistical significance was determined by unpaired Student's t test. * $p < 0.05$; ** $p < 0.01$; *** $p < 0.001$, **** $p < 0.0001$.

Figure S1. TCF1 deficiency selectively reprograms T_{reg}s without compromising their core signature. (a) Representative FACS histograms of MLN purified cells from *Tcf7*$^{fl/fl}$ *Foxp3*^{Cre} and control *Foxp3*^{Cre} showing selective loss of Tcf1 from T_{reg}s of *Tcf7*$^{fl/fl}$ *Foxp3*^{Cre} mice. (**b** and **c**) Histogram plots showing the cumulative data of the same. (**d**) GSEA plot comparing the enrichment of genes expressed more highly in Tcf1-sufficient (*Foxp3*^{Cre}) versus Tcf1-deficient (*Tcf7*$^{fl/fl}$ *Foxp3*^{Cre}) T_{reg}s.

Figure S2. Schematic representation of magnetic purification of T_{reg}s, and FACS analysis showing over 90% purity.

Figure S3. Single-cell RNAseq reveals distinct T_{reg} populations. (**a**) mRNA expression of select indicated genes projected on the UMAP. (**b**) Map showing observed (cells on the UMAP) and extrapolated future state of cells (overlaid arrows) based on RNA velocity.

Figure S4. TCF1-deficient and sufficient T_{reg}s show distinct effector functions. mRNA expression of Erdr1 and Igfbp4 projected on the UMAP.

Figure S5. (**a**) UMAP projection (left) and fraction of cells in each cell type (stack bars; right panel) for APC$^{\Delta 486}$ and control B6 T_{reg}s. Data are from two replicates. (**b**) Dot plot showing the expression of TCF1 across all cell types in *Apc*$^{\Delta 486}$ and control *B6* T_{reg}s. Color and size of the dots are proportional to the expression level and percent of cells expressing Tcf1 in each indicated cluster. (**c**) Expression of differentially expressed genes, *Socs3*, *Jund* and *Lag3* between *APC*$^{\Delta 486}$ and *B6* cells projected on the UMAP. See TableS4 for the full list. (**d**) Expression changes of the most differentially expressed genes between *Apc*^{486} and control *B6* T_{reg}s. See TableS4 for the full list. The fold change in expression intensities is color-coded. The fold change in percent of cells expressing the indicated gene in each cell type is proportional to the circle size. Adjusted-p-values > 0.01 are masked with gray color. (**e**) RNA velocity vectors overlaid on UMAP for *B6* (left) and *Apc*$^{\Delta 486}$ (right) T_{reg}s.

Figure1

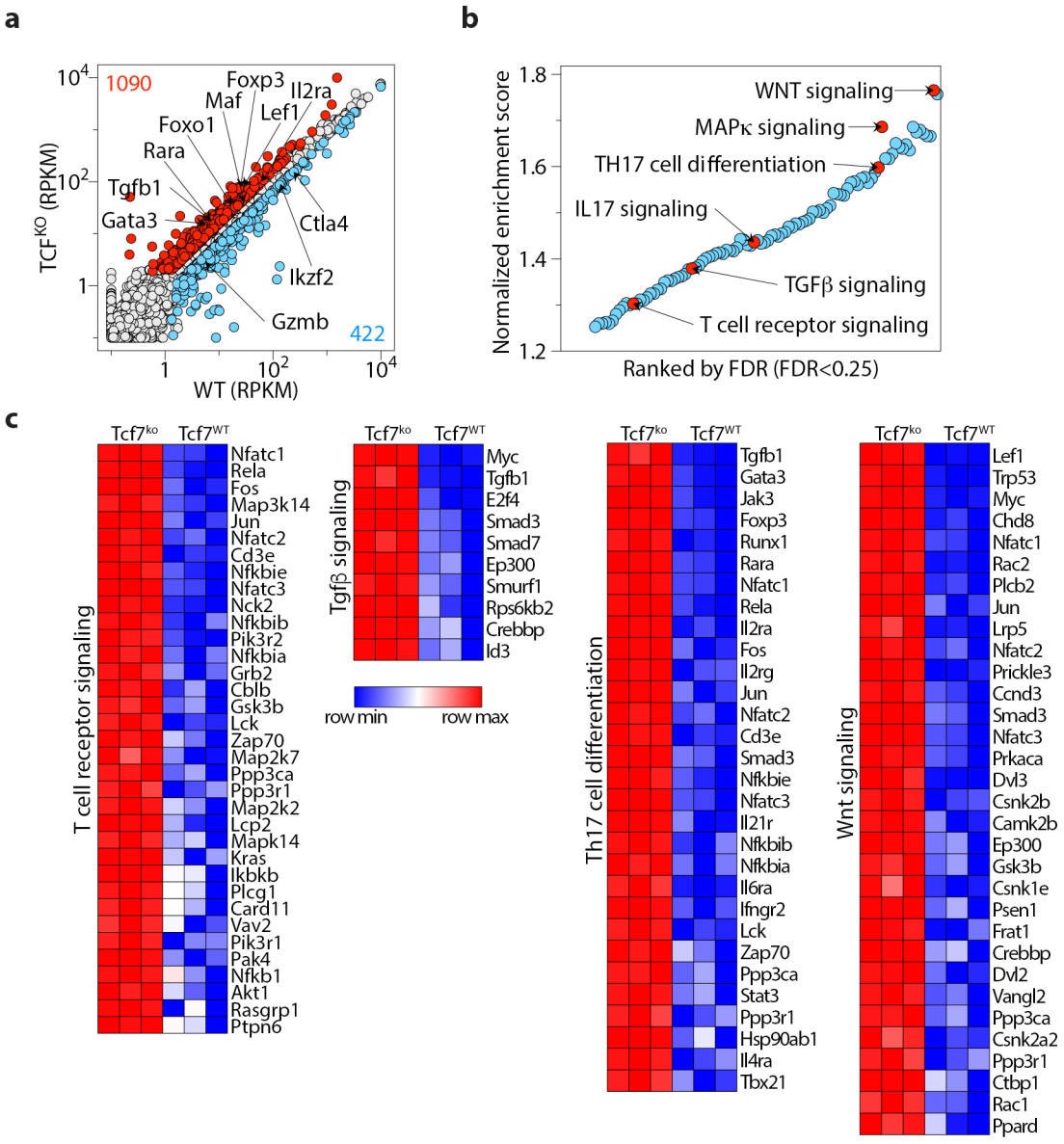
a
b
c
1090
422
Foxp3
Il2ra
Maf
Lef1
Foxo1
Rara
Tgfb1
Gata3
Ctla4
Ikzf2
Gzmb
TCF^KO (RPKM)
WT (RPKM)
WNT signaling
MAPκ signaling
TH17 cell differentiation
IL17 signaling
TGFβ signaling
T cell receptor signaling
Normalized enrichment score
Ranked by FDR (FDR<0.25)
Tcf7ko
Tcf7WT
T cell receptor signaling
Nfatc1
Rela
Fos
Map3k14
Jun
Nfatc2
Cd3e
Nfkbie
Nfatc3
Nck2
Nfkbib
Pik3r2
Nfkbia
Grb2
Cblb
Gsk3b
Lck
Zap70
Map2k7
Ppp3ca
Ppp3r1
Map2k2
Lcp2
Mapk14
Kras
Ikbkb
Plcg1
Card11
Vav2
Pik3r1
Pak4
Nfkb1
Akt1
Rasgrp1
Ptpn6
Tgfβ signaling
Myc
Tgfb1
E2f4
Smad3
Smad7
Ep300
Smurf1
Rps6kb2
Crebbp
Id3
row min
row max
Th17 cell differentiation
Tgfb1
Gata3
Jak3
Foxp3
Runx1
Rara
Nfatc1
Rela
Il2ra
Fos
Il2rg
Jun
Nfatc2
Cd3e
Smad3
Nfkbie
Nfatc3
Il21r
Nfkbib
Nfkbia
Il6ra
Ifngr2
Lck
Zap70
Ppp3ca
Stat3
Ppp3r1
Hsp90ab1
Il4ra
Tbx21
Wnt signaling
Lef1
Trp53
Myc
Chd8
Nfatc1
Rac2
Plcb2
Jun
Lrp5
Nfatc2
Prickle3
Ccnd3
Smad3
Nfatc3
Prkaca
Dvl3
Csnk2b
Camk2b
Ep300
Gsk3b
Csnk1e
Psen1
Frat1
Crebbp
Dvl2
Vangl2
Ppp3ca
Csnk2a2
Ppp3r1
Ctbp1
Rac1
Ppard

Figure2

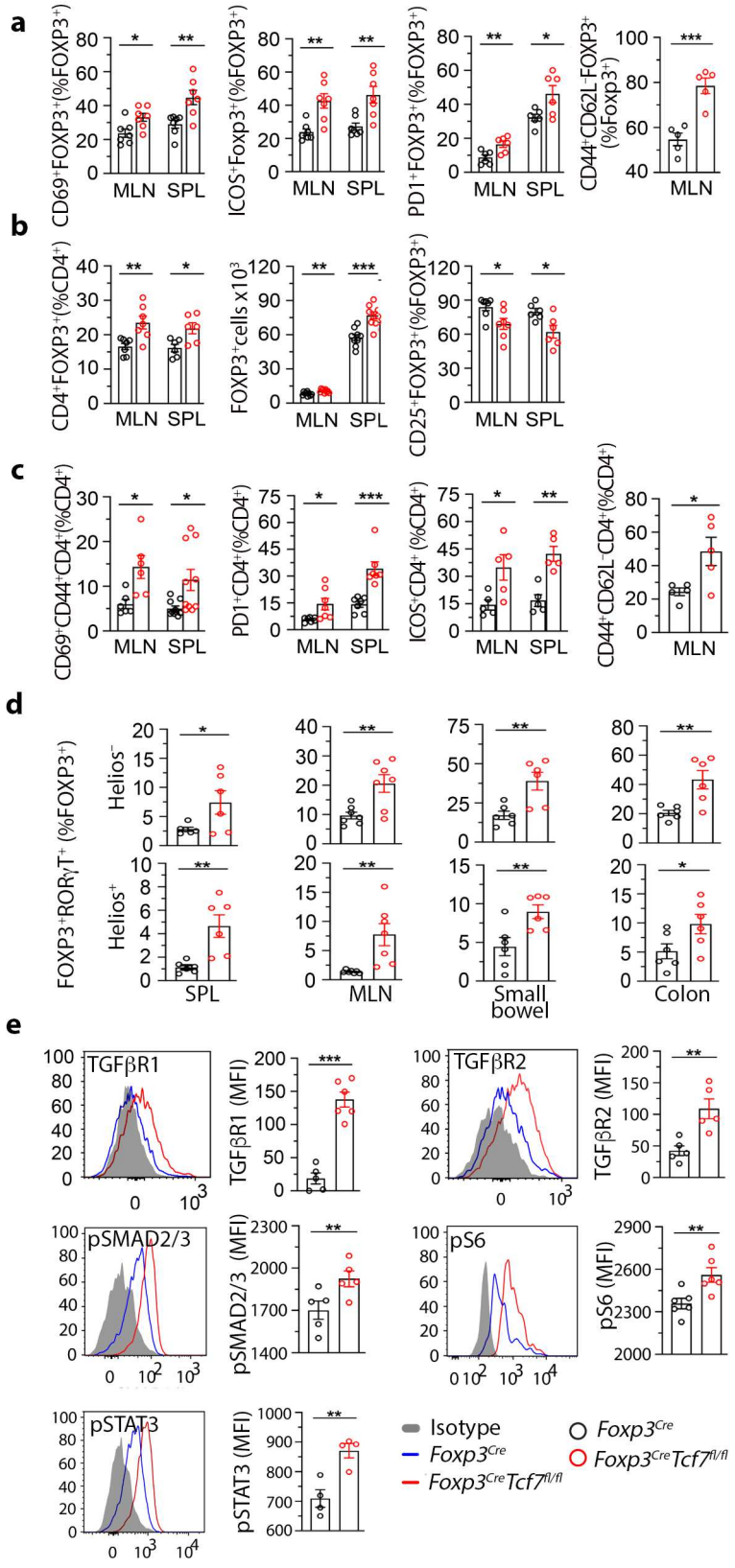
a
CD69+FOXP3+(%FOXP3+)
ICOS+Foxp3+(%FOXP3+)
PD1+FOXP3+(%FOXP3+)
CD44+CD62L-FOXP3+ (%Foxp3+)
MLN SPL
b
CD4+FOXP3+(%CD4+)
FOXP3+cells x10^3
CD25+FOXP3+(%FOXP3+)
c
CD69+CD44+CD4+(%CD4+)
PD1+CD4+(%CD4+)
ICOS+CD4+ (%CD4+)
CD44+CD62L-CD4+(%CD4+)
d
FOXP3+RORγT+ (%FOXP3+)
Helios-
Helios+
SPL
MLN
Small bowel
Colon
e
TGFβR1
TGFβR1 (MFI)
TGFβR2
TGFβR2 (MFI)
pSMAD2/3
pSMAD2/3 (MFI)
pS6
pS6 (MFI)
pSTAT3
pSTAT3 (MFI)
Isotype
Foxp3Cre
Foxp3CreTcf7fl/fl
Foxp3Cre
Foxp3CreTcf7fl/fl

Figure3

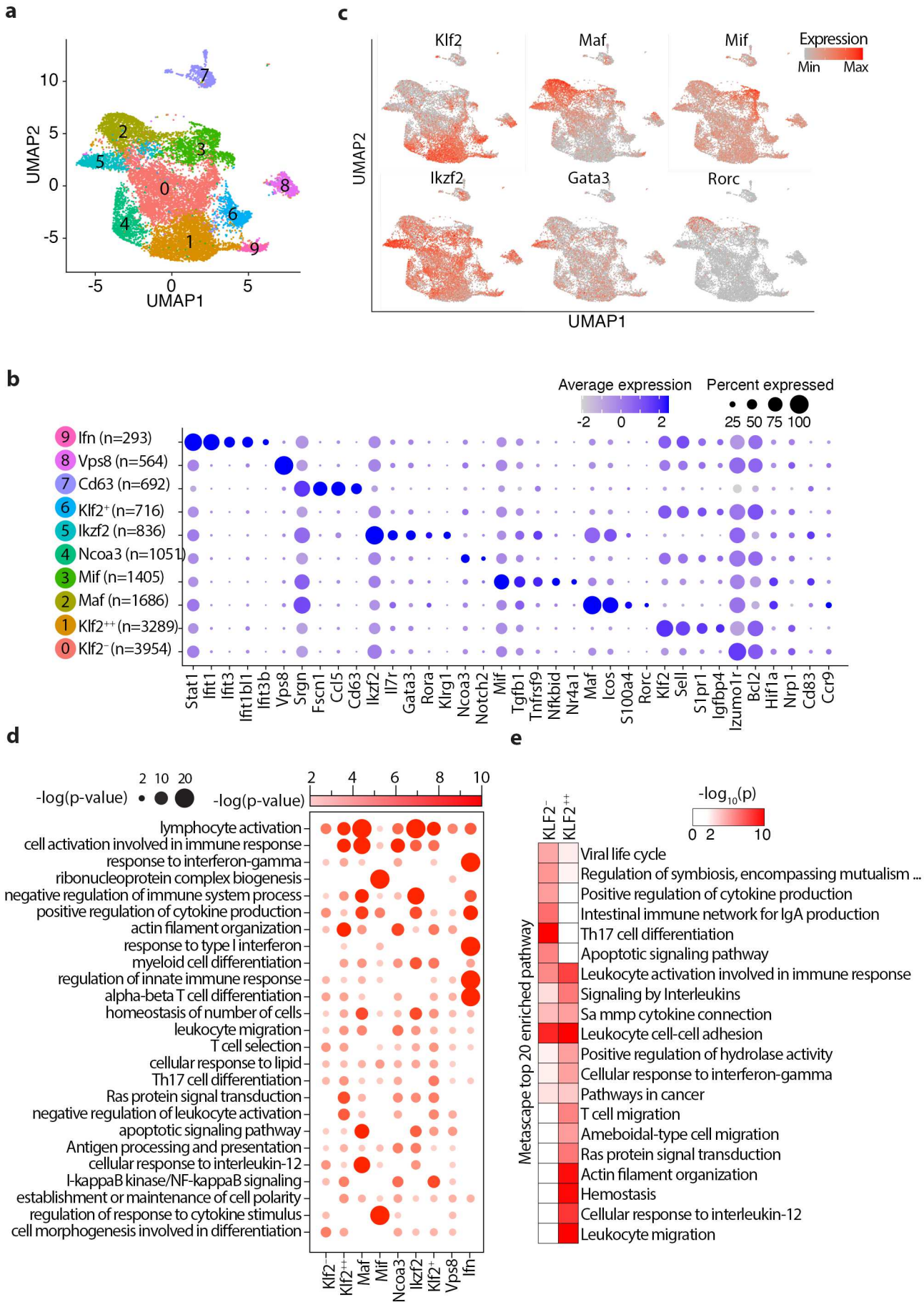
a
UMAP2
UMAP1
c
Klf2
Maf
Mif
Ikzf2
Gata3
Rorc
Expression
Min
Max
UMAP2
UMAP1
b
Average expression
Percent expressed
9 Ifn (n=293)
8 Vps8 (n=564)
7 Cd63 (n=692)
6 Klf2+ (n=716)
5 Ikzf2 (n=836)
4 Ncoa3 (n=1051)
3 Mif (n=1405)
2 Maf (n=1686)
1 Klf2++ (n=3289)
0 Klf2- (n=3954)
Stat1 Ifit1 Ifit3 Ifit1bl1 Ifit3b Vps8 Srgn Fscn1 Ccl5 Cd63 Ikzf2 Il7r Gata3 Rora Klrg1 Ncoa3 Notch2 Mif Tgfb1 Tnfrsf9 Nfkbid Nr4a1 Maf Icos S100a4 Rorc Klf2 Sell S1pr1 Igfbp4 Izumo1r Bcl2 Hif1a Nrp1 Cd83 Ccr9
d
-log(p-value)
lymphocyte activation
cell activation involved in immune response
response to interferon-gamma
ribonucleoprotein complex biogenesis
negative regulation of immune system process
positive regulation of cytokine production
actin filament organization
response to type I interferon
myeloid cell differentiation
regulation of innate immune response
alpha-beta T cell differentiation
homeostasis of number of cells
leukocyte migration
T cell selection
cellular response to lipid
Th17 cell differentiation
Ras protein signal transduction
negative regulation of leukocyte activation
apoptotic signaling pathway
Antigen processing and presentation
cellular response to interleukin-12
I-kappaB kinase/NF-kappaB signaling
establishment or maintenance of cell polarity
regulation of response to cytokine stimulus
cell morphogenesis involved in differentiation
Klf2- Klf2++ Maf Mif Ncoa3 Ikzf2 Klf2+ Vps8 Ifn
e
-log10(p)
KLF2- KLF2++
Metascape top 20 enriched pathway
Viral life cycle
Regulation of symbiosis, encompassing mutualism ...
Positive regulation of cytokine production
Intestinal immune network for IgA production
Th17 cell differentiation
Apoptotic signaling pathway
Leukocyte activation involved in immune response
Signaling by Interleukins
Sa mmp cytokine connection
Leukocyte cell-cell adhesion
Positive regulation of hydrolase activity
Cellular response to interferon-gamma
Pathways in cancer
T cell migration
Ameboidal-type cell migration
Ras protein signal transduction
Actin filament organization
Hemostasis
Cellular response to interleukin-12
Leukocyte migration

Figure4

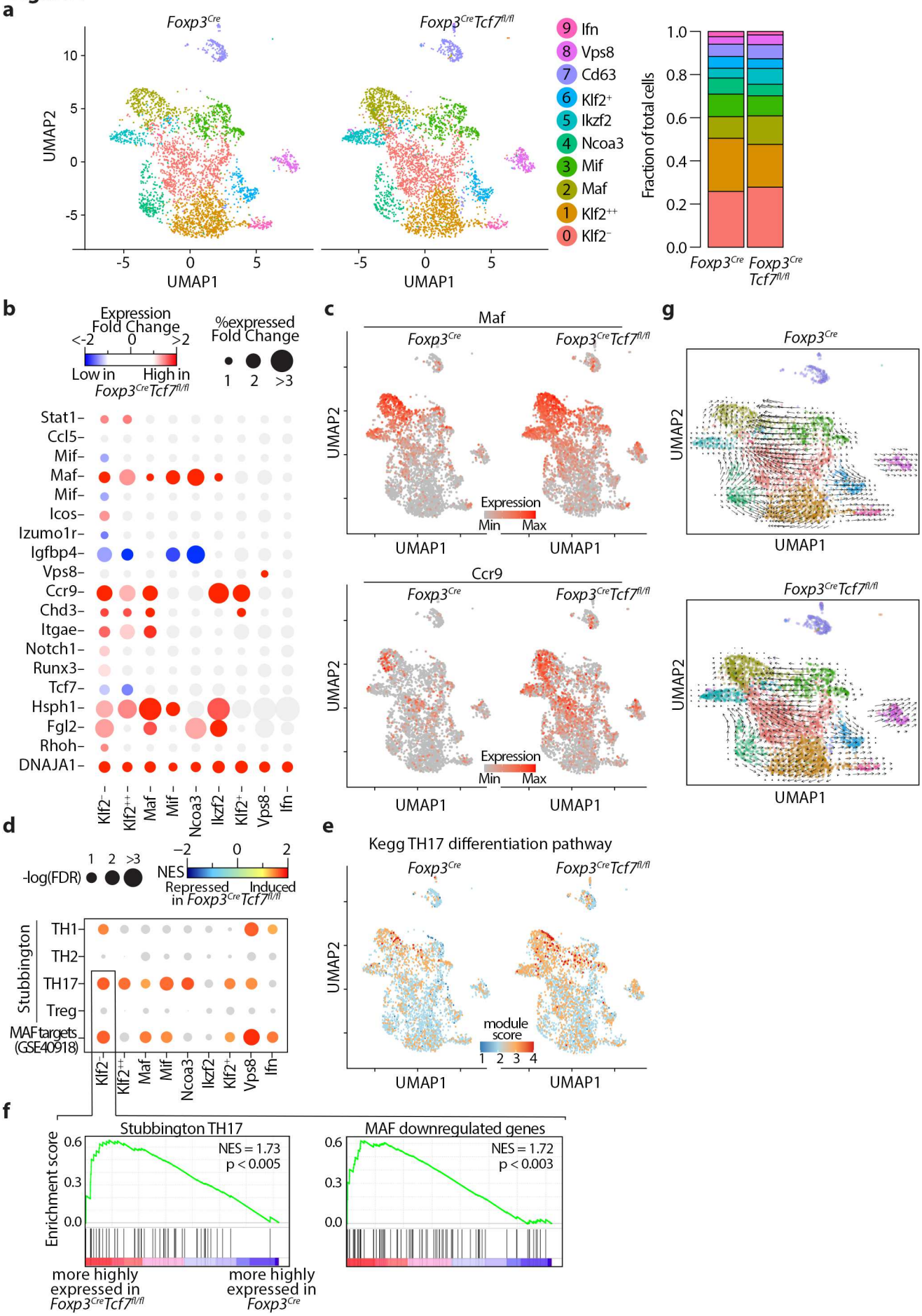
a
Foxp3Cre
Foxp3CreTcf7fl/fl
UMAP1
UMAP2
9 Ifn
8 Vps8
7 Cd63
6 Klf2+
5 Ikzf2
4 Ncoa3
3 Mif
2 Maf
1 Klf2++
0 Klf2−
Fraction of total cells
b
Expression Fold Change
%expressed Fold Change
Low in Foxp3CreTcf7fl/fl
High in
Stat1
Ccl5
Mif
Maf
Mif
Icos
Izumo1r
Igfbp4
Vps8
Ccr9
Chd3
Itgae
Notch1
Runx3
Tcf7
Hsph1
Fgl2
Rhoh
DNAJA1
c
Maf
Ccr9
Expression
Min
Max
g
d
-log(FDR)
NES
Repressed in Foxp3CreTcf7fl/fl
Induced
Stubbington
TH1
TH2
TH17
Treg
MAF targets (GSE40918)
e
Kegg TH17 differentiation pathway
module score
f
Stubbington TH17
MAF downregulated genes
Enrichment score
NES = 1.73
p < 0.005
NES = 1.72
p < 0.003
more highly expressed in Foxp3CreTcf7fl/fl
more highly expressed in Foxp3Cre

Figure5

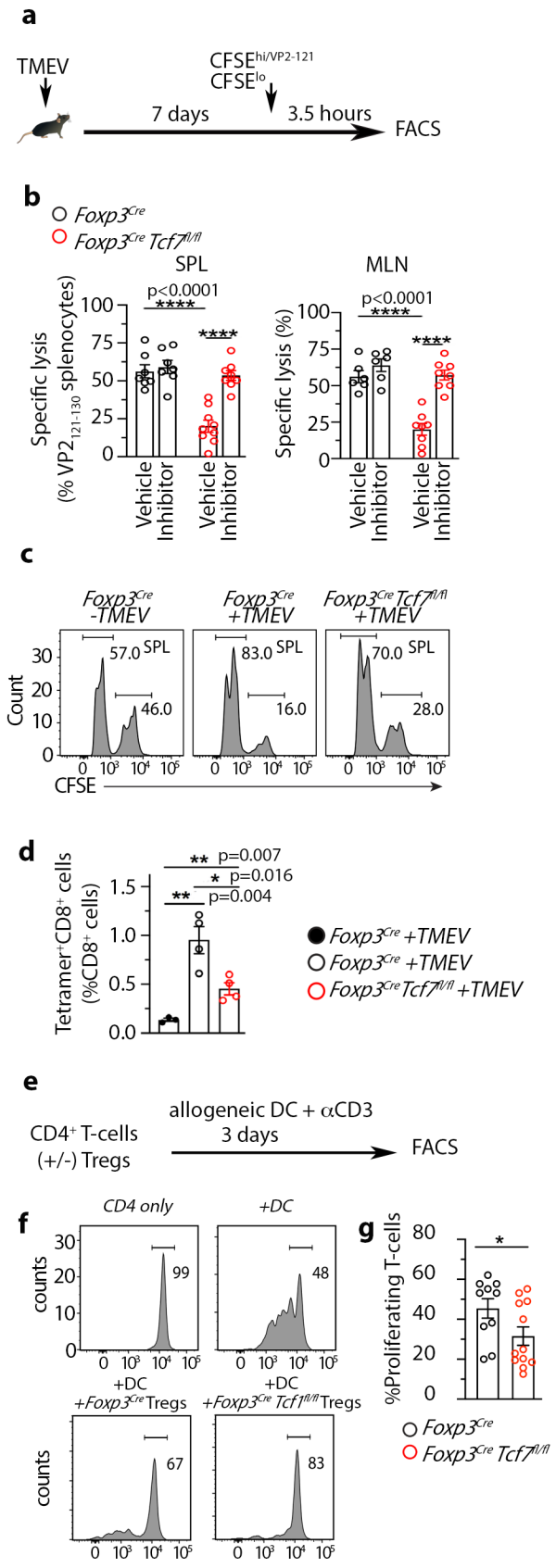
a
TMEV
CFSE^hi/VP2-121
CFSE^lo
7 days
3.5 hours
FACS
b
Foxp3^Cre
Foxp3^Cre Tcf7^fl/fl
SPL
MLN
p<0.0001
****
Specific lysis (% VP2 121-130 splenocytes)
Specific lysis (%)
Vehicle
Inhibitor
c
Foxp3^Cre -TMEV
Foxp3^Cre +TMEV
Foxp3^Cre Tcf7^fl/fl +TMEV
57.0 SPL
46.0
83.0 SPL
16.0
70.0 SPL
28.0
Count
CFSE
d
** p=0.007
* p=0.016
** p=0.004
Tetramer+CD8+ cells (%CD8+ cells)
Foxp3^Cre +TMEV
Foxp3^Cre +TMEV
Foxp3^Cre Tcf7^fl/fl +TMEV
e
CD4+ T-cells
(+/-) Tregs
allogeneic DC + αCD3
3 days
FACS
f
CD4 only
+DC
99
48
counts
+DC
+Foxp3^Cre Tregs
+DC
+Foxp3^Cre Tcf1^fl/fl Tregs
67
83
g
%Proliferating T-cells
*
Foxp3^Cre
Foxp3^Cre Tcf7^fl/fl

Figure6

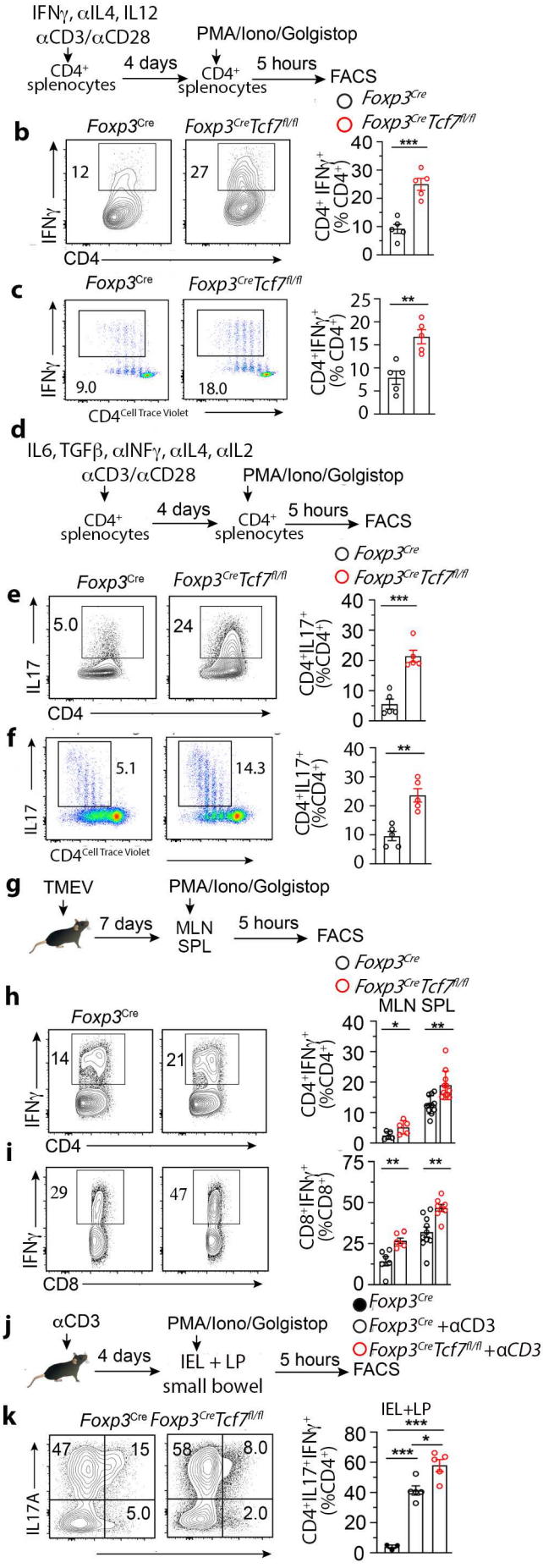
IFNγ, αIL4, IL12
αCD3/αCD28
CD4+ splenocytes
4 days
PMA/Iono/Golgistop
CD4+ splenocytes
5 hours
FACS
Foxp3Cre
Foxp3CreTcf7fl/fl
b
Foxp3Cre
Foxp3CreTcf7fl/fl
12
27
IFNγ
CD4
CD4+ IFNγ+ (% CD4+)
***
c
Foxp3Cre
Foxp3CreTcf7fl/fl
9.0
18.0
IFNγ
CD4Cell Trace Violet
CD4+IFNγ+ (% CD4+)
**
d
IL6, TGFβ, αINFγ, αIL4, αIL2
αCD3/αCD28
PMA/Iono/Golgistop
CD4+ splenocytes
4 days
CD4+ splenocytes
5 hours
FACS
Foxp3Cre
Foxp3CreTcf7fl/fl
e
Foxp3Cre
Foxp3CreTcf7fl/fl
5.0
24
IL17
CD4
CD4+IL17+ (%CD4+)
***
f
5.1
14.3
IL17
CD4Cell Trace Violet
CD4+IL17+ (%CD4+)
**
g
TMEV
7 days
PMA/Iono/Golgistop
MLN SPL
5 hours
FACS
Foxp3Cre
Foxp3CreTcf7fl/fl
h
Foxp3Cre
14
21
IFNγ
CD4
MLN SPL
CD4+IFNγ+ (%CD4+)
*
**
i
29
47
IFNγ
CD8
CD8+IFNγ+ (%αCD8+)
**
**
Foxp3Cre
j
αCD3
4 days
PMA/Iono/Golgistop
IEL + LP
small bowel
5 hours
FACS
Foxp3Cre +αCD3
Foxp3CreTcf7fl/fl +αCD3
k
Foxp3Cre Foxp3CreTcf7fl/fl
47
15
5.0
58
8.0
2.0
IL17A
IEL+LP
CD4+IL17+IFNγ+ (%CD4+)
***
*
***

Figure7

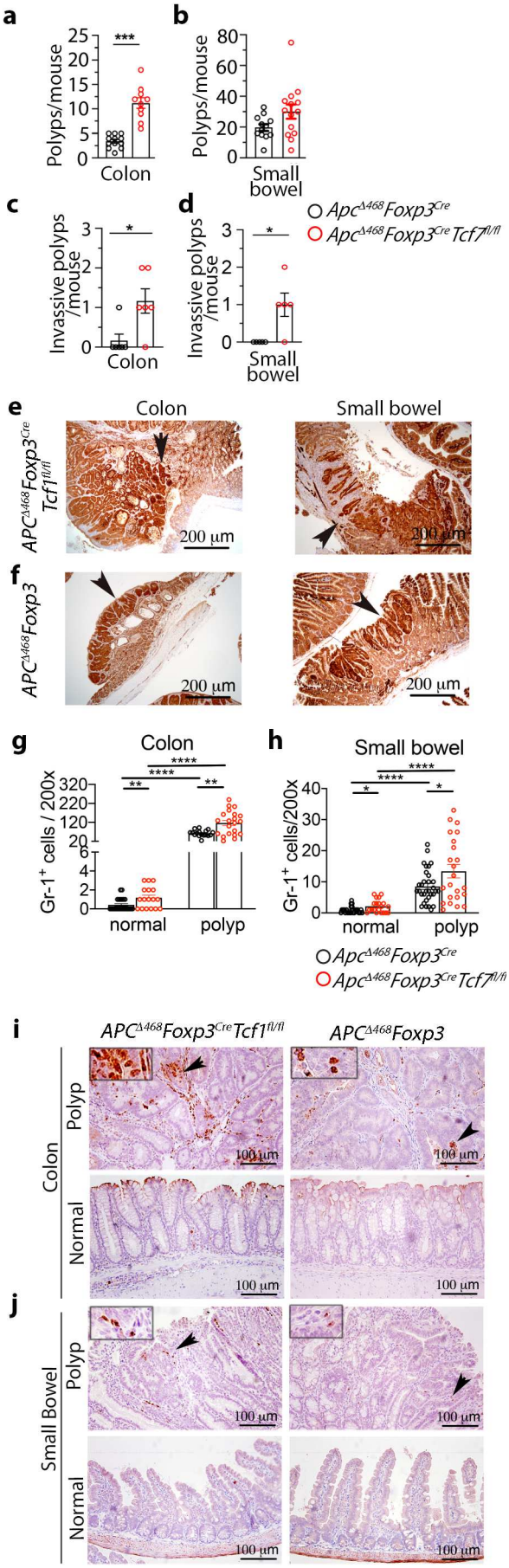
a
Polyps/mouse
***
Colon
b
Polyps/mouse
Small bowel
c
Invassive polyps /mouse
*
Colon
d
Invassive polyps /mouse
*
Small bowel
APCΔ468Foxp3Cre
APCΔ468Foxp3CreTcf7fl/fl
e
Colon
Small bowel
APCΔ468Foxp3CreTcf1fl/fl
200 μm
f
APCΔ468Foxp3
200 μm
g
Colon
Gr-1+ cells / 200x
normal
polyp
h
Small bowel
Gr-1+ cells/200x
normal
polyp
APCΔ468Foxp3Cre
APCΔ468Foxp3CreTcf7fl/fl
i
APCΔ468Foxp3CreTcf1fl/fl
APCΔ468Foxp3
Colon
Polyp
Normal
100 μm
j
Small Bowel
Polyp
Normal
100 μm

FigureS1

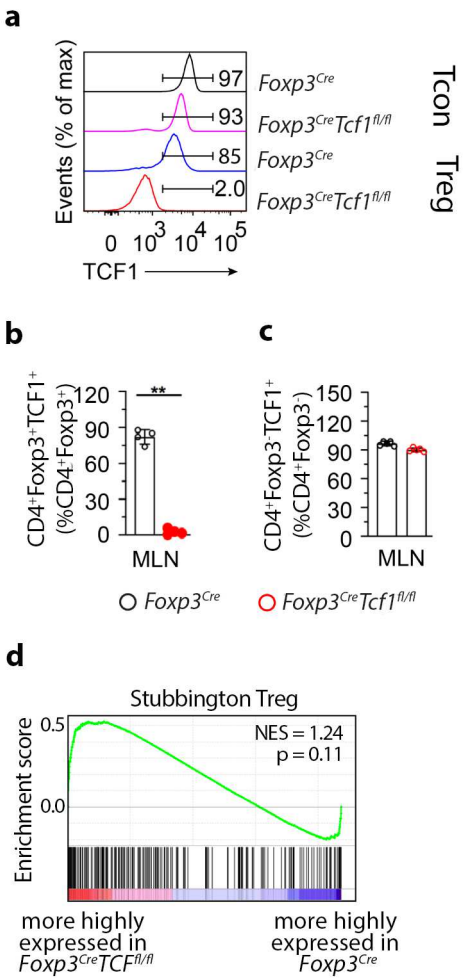
a
Events (% of max)
97
93
85
2.0
Foxp3Cre
Foxp3CreTcf1fl/fl
Foxp3Cre
Foxp3CreTcf1fl/fl
Tcon
Treg
0 10^3 10^4 10^5
TCF1
b
CD4+Foxp3+TCF1+ (%CD4+Foxp3+)
120
90
60
30
0
**
MLN
Foxp3Cre
c
CD4+Foxp3-TCF1+ (%CD4+Foxp3-)
150
120
90
60
30
0
MLN
Foxp3CreTcf1fl/fl
d
Stubbington Treg
Enrichment score
0.5
0.0
NES = 1.24
p = 0.11
more highly expressed in Foxp3CreTCFfl/fl
more highly expressed in Foxp3Cre

FigureS2

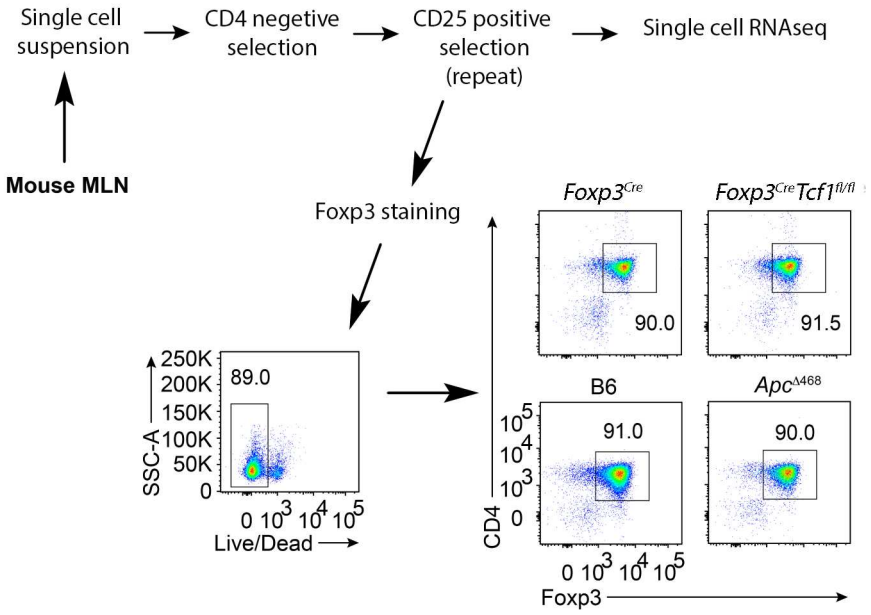
Single cell suspension
CD4 negetive selection
CD25 positive selection (repeat)
Single cell RNAseq
Mouse MLN
Foxp3 staining
Foxp3^Cre
Foxp3^CreTcf1^fl/fl
90.0
91.5
250K
200K
150K
100K
50K
0
89.0
SSC-A
0 10^3 10^4 10^5
Live/Dead
B6
Apc^Δ468
10^5
10^4
10^3
0
91.0
90.0
CD4
0 10^3 10^4 10^5
Foxp3

FigureS3

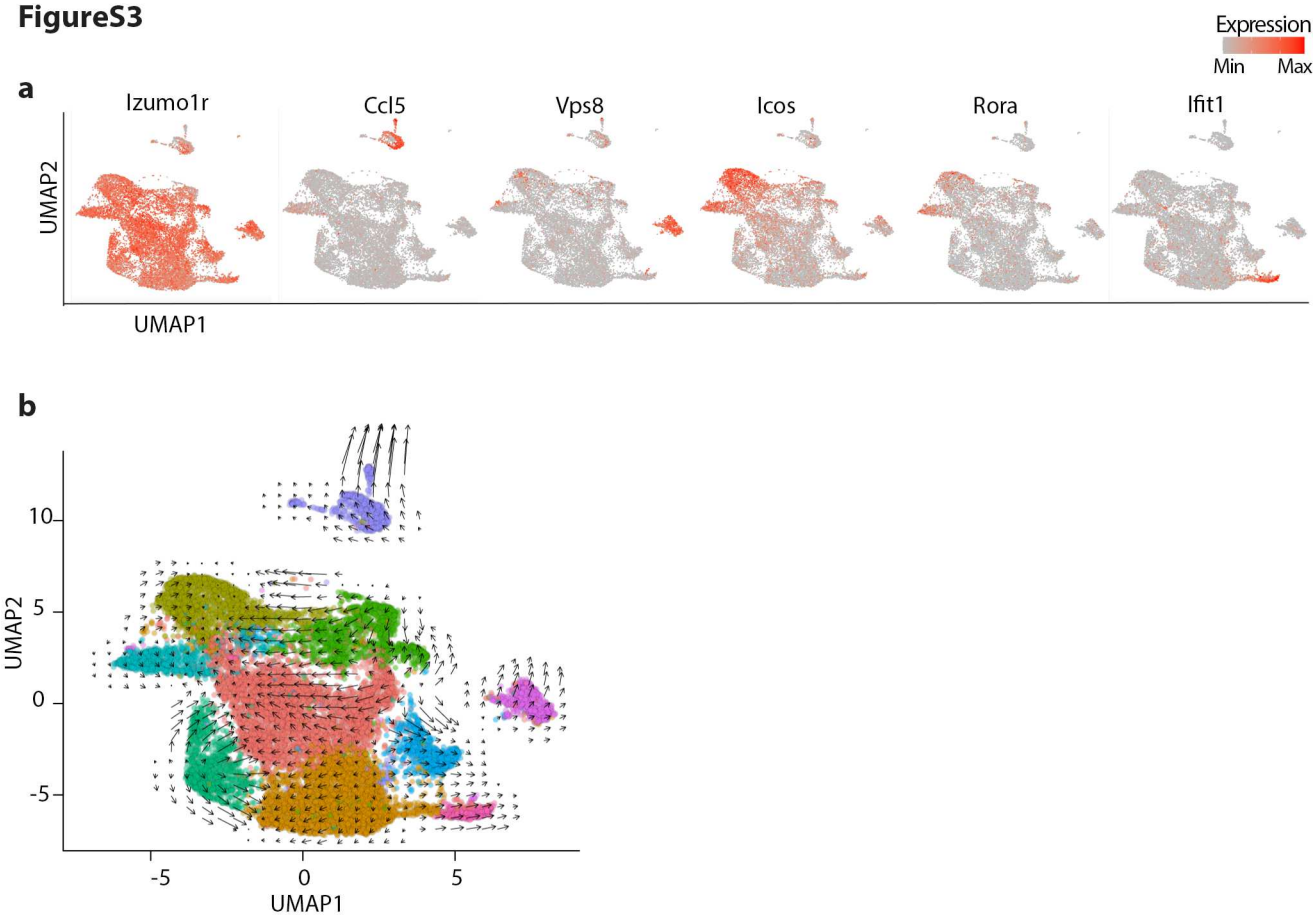
a
Izumo1r
Ccl5
Vps8
Icos
Rora
Ifit1
Expression
Min
Max
UMAP2
UMAP1
b
10
5
0
-5
UMAP2
-5
0
5
UMAP1

FigureS4

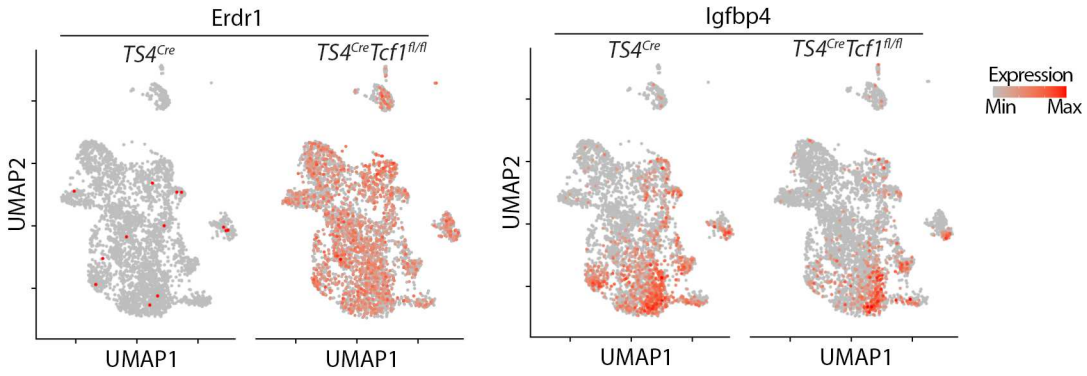
Erdr1
TS4Cre
TS4CreTcf1fl/fl
UMAP2
UMAP1
UMAP1
Igfbp4
TS4Cre
TS4CreTcf1fl/fl
UMAP2
UMAP1
UMAP1
Expression
Min
Max

FigureS5

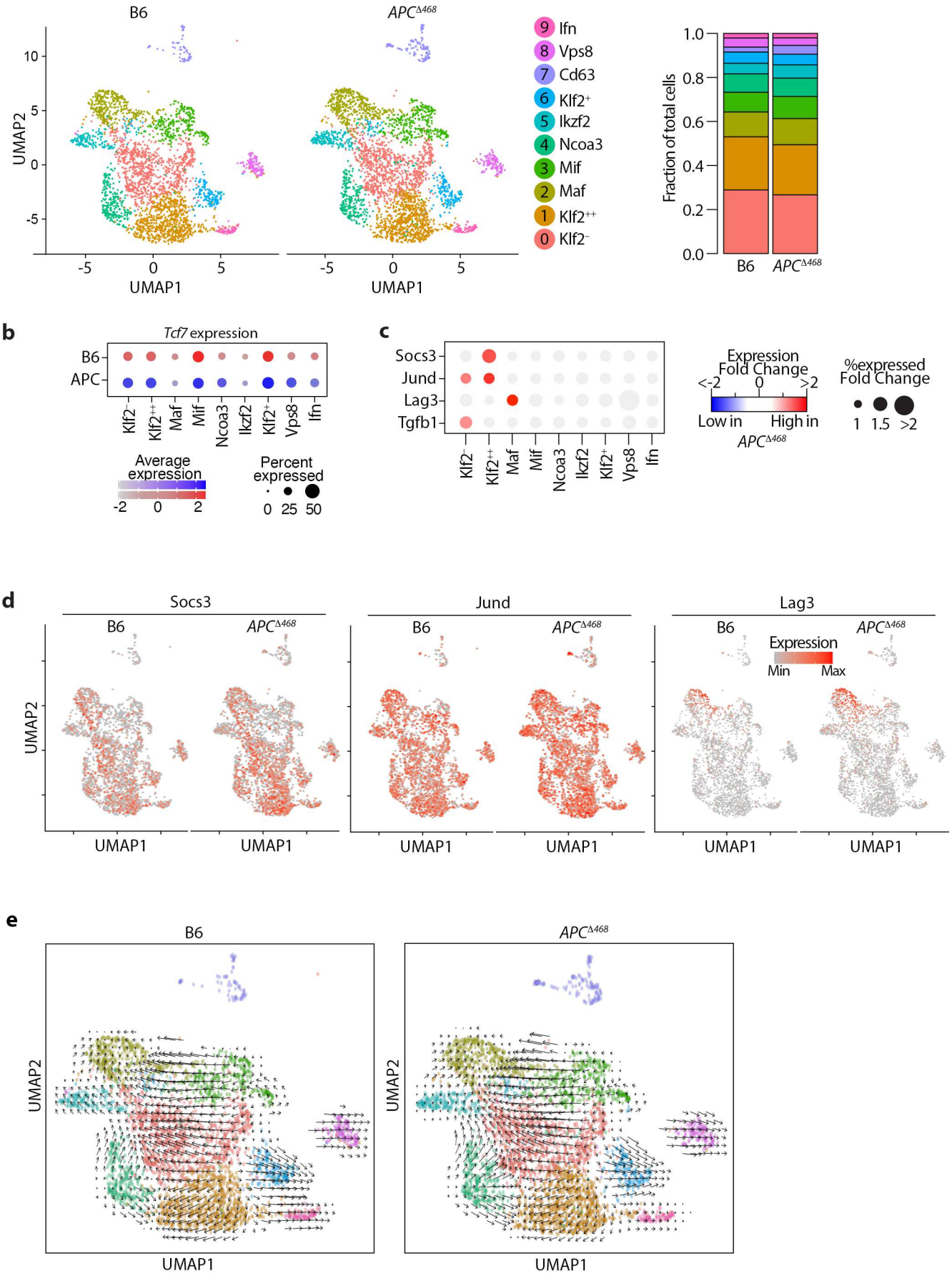
B6
APC^Δ468
UMAP2
UMAP1
9 Ifn
8 Vps8
7 Cd63
6 Klf2+
5 Ikzf2
4 Ncoa3
3 Mif
2 Maf
1 Klf2++
0 Klf2−
Fraction of total cells
b
Tcf7 expression
Average expression
Percent expressed
c
Socs3
Jund
Lag3
Tgfb1
Expression Fold Change
%expressed Fold Change
Low in
High in
d
Expression
Min
Max
e

Figures

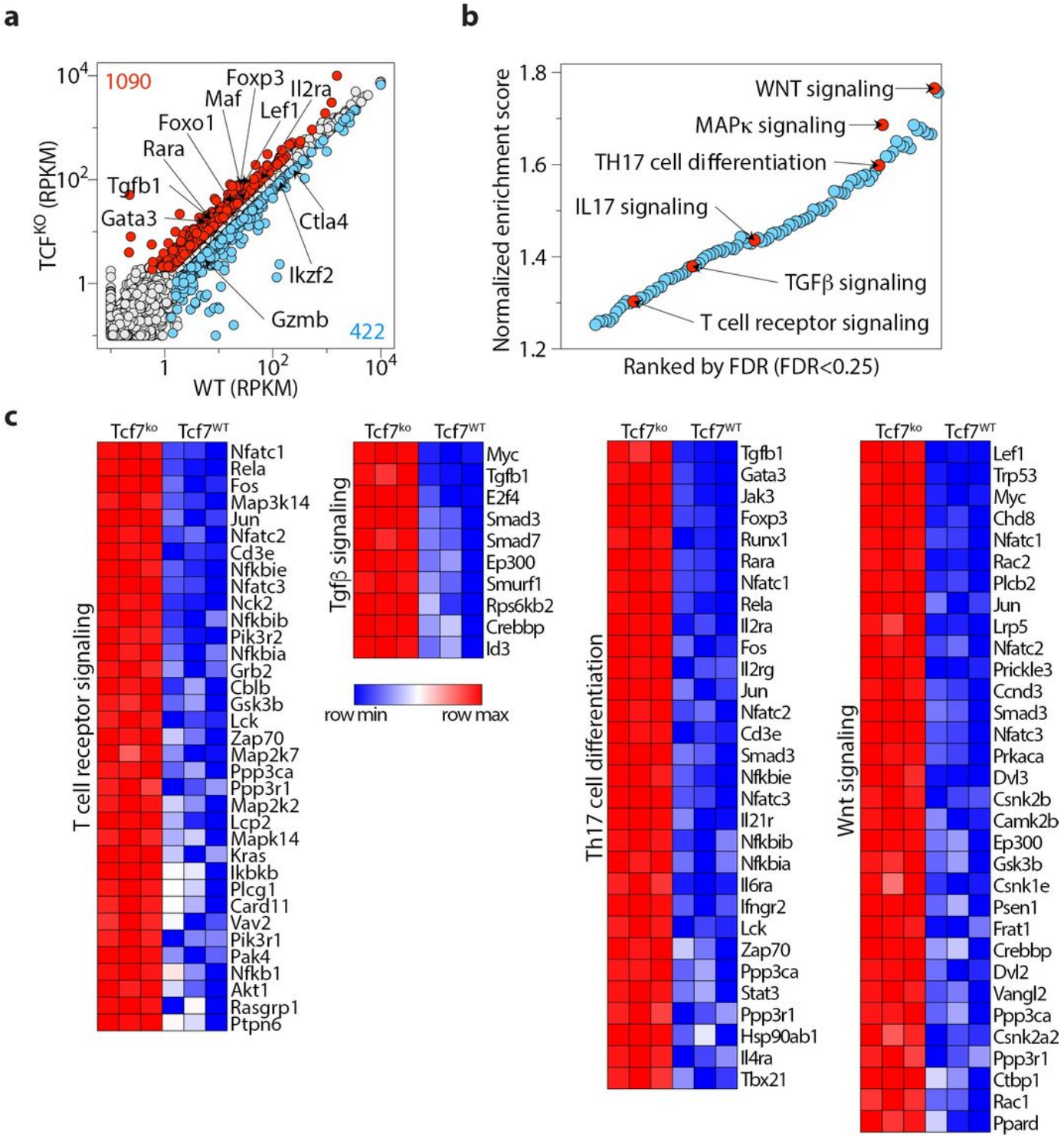

Figure 1

TCF1 deficiency selectively reprograms Tregs without compromising their core signature. (a) Scatter plot comparing the expression of genes in TCF1-sufficient (Foxp3Cre) and TCF1-deficient (Foxp3Cre Tcf7fl/fl) Tregs. Reads Per Kilobase of transcript, per Million mapped reads (RPKM) expression values are

average of three biological replicates. Significantly up- or downregulated genes (fold change >1.5 and FDR < 0.001) are shown in red or blue with exact numbers shown at the top or bottom corner, respectively. (b) Significantly enriched Kegg pathways by gene set enrichment analysis (GSEA) induced in transcriptomes of Tcf1-deficient versus sufficient Tregs. Normalized enrichment scores of all enriched Kegg pathways (FDR< 25%) are shown. Select pathways are highlighted. See TableS1 for the full list. (c) The expression of all leading-edge genes from four indicated pathways.

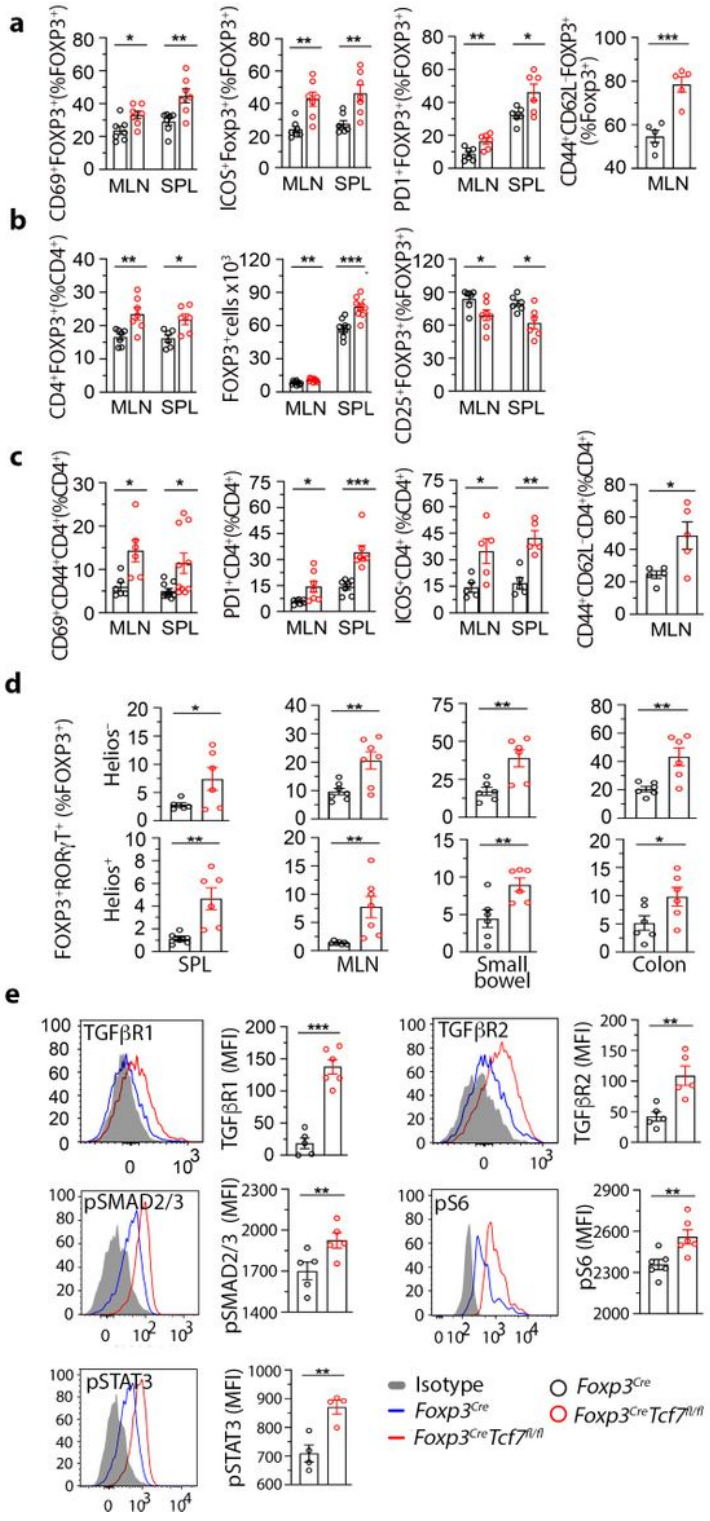

Figure 2

Cumulative data from FACS analysis shows activation and expansion of Tregs and Teff cells in TCF1-deficient mice. Tregs and CD4+ Teff cells from 5.5-month-old Foxp3Cre Tcf7fl/fl mice and control Foxp3Cre mice were analyzed by FACS. (a) Frequency of CD4+Foxp3+ Tregs expressing CD69, ICOS, PD-1, and CD44 and CD62L, in MLN and spleen. (b) Treg frequency and numbers and expression of CD25 in the MLN and spleen. (c) Frequency of conventional CD4+ T-cells expressing CD69, PD-1, ICOS, and CD44 and CD62L, in MLN and spleen. (d) The frequency of HELIOS- or HELIOS+FOXP3+RORγT+ Tregs, in the spleen, MLN, small bowel, and colon. (e) Representative FACS histograms normalized to mode (left) and bar diagrams of cumulative data for expression of TGFbR1, TGFbR2, pSMAD2/3, pS6, and pSTAT5 by Tregs. For the cumulative data, each symbol represents a value from an individual mouse. Data are means ± SEM unpaired Student's t test. * $p < 0.05$; ** $p < 0.01$; *** $p < 0.001$.

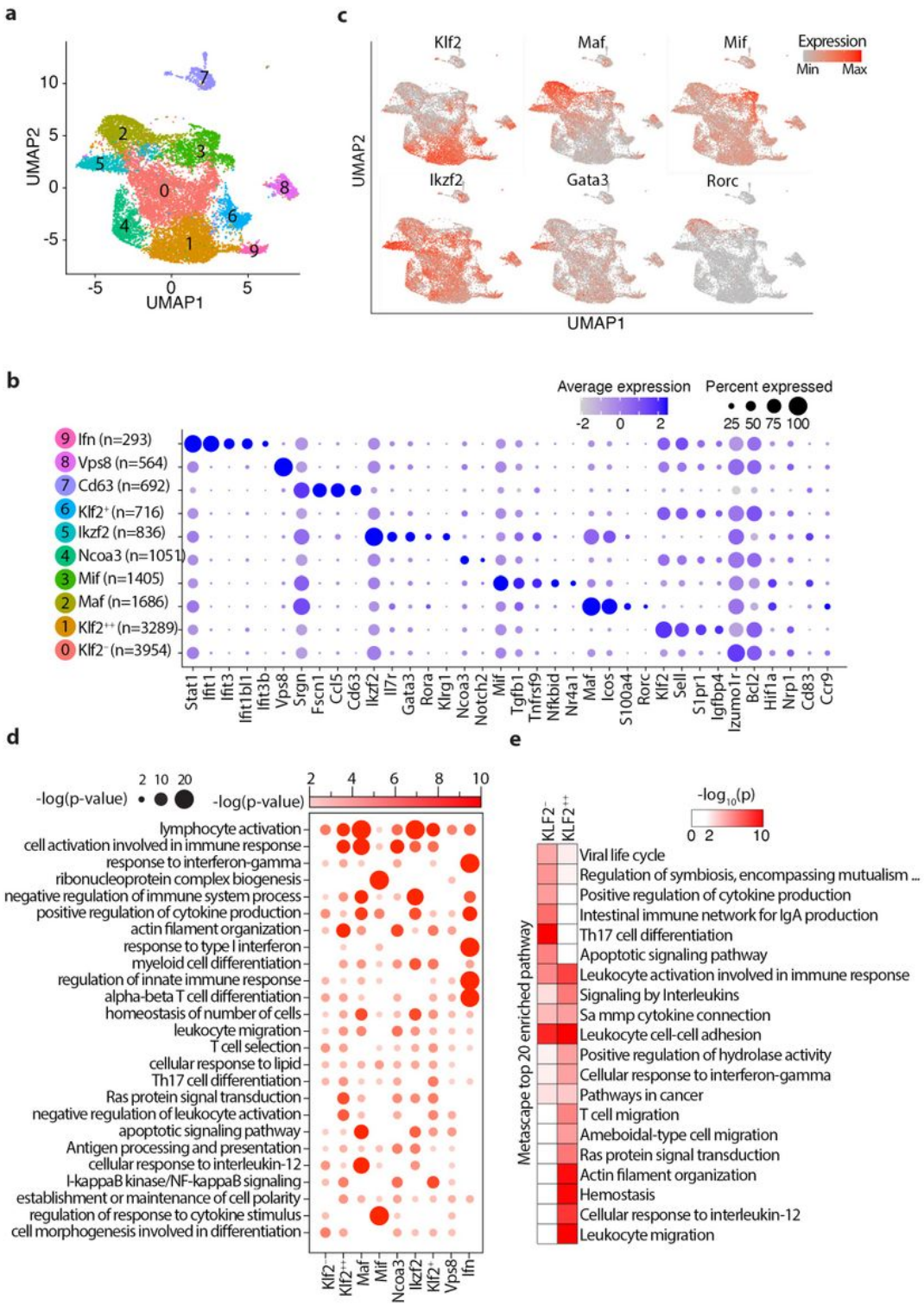

Figure 3

Single cell transcriptomics delineate distinct Treg subpopulations in the mesenteric lymph nodes. (a) Integrated UMAP showing 10 major cell types in isolated Tregs from mice used in this study. (b) Expression of cell-defining features across all cell types. (c) mRNA expression of select indicated genes projected on the UMAP. (d) Significantly enriched pathways by Metascape based on top 200 genes upregulated in indicated cell type compared to all other cell types. See TableS2 for the full list. (e) 20

most significantly enriched pathways by Metascape based on genes upregulated in Klf2– or Klf2++ cell types compared directly to Klf2++ or Klf2– cell types, respectively.

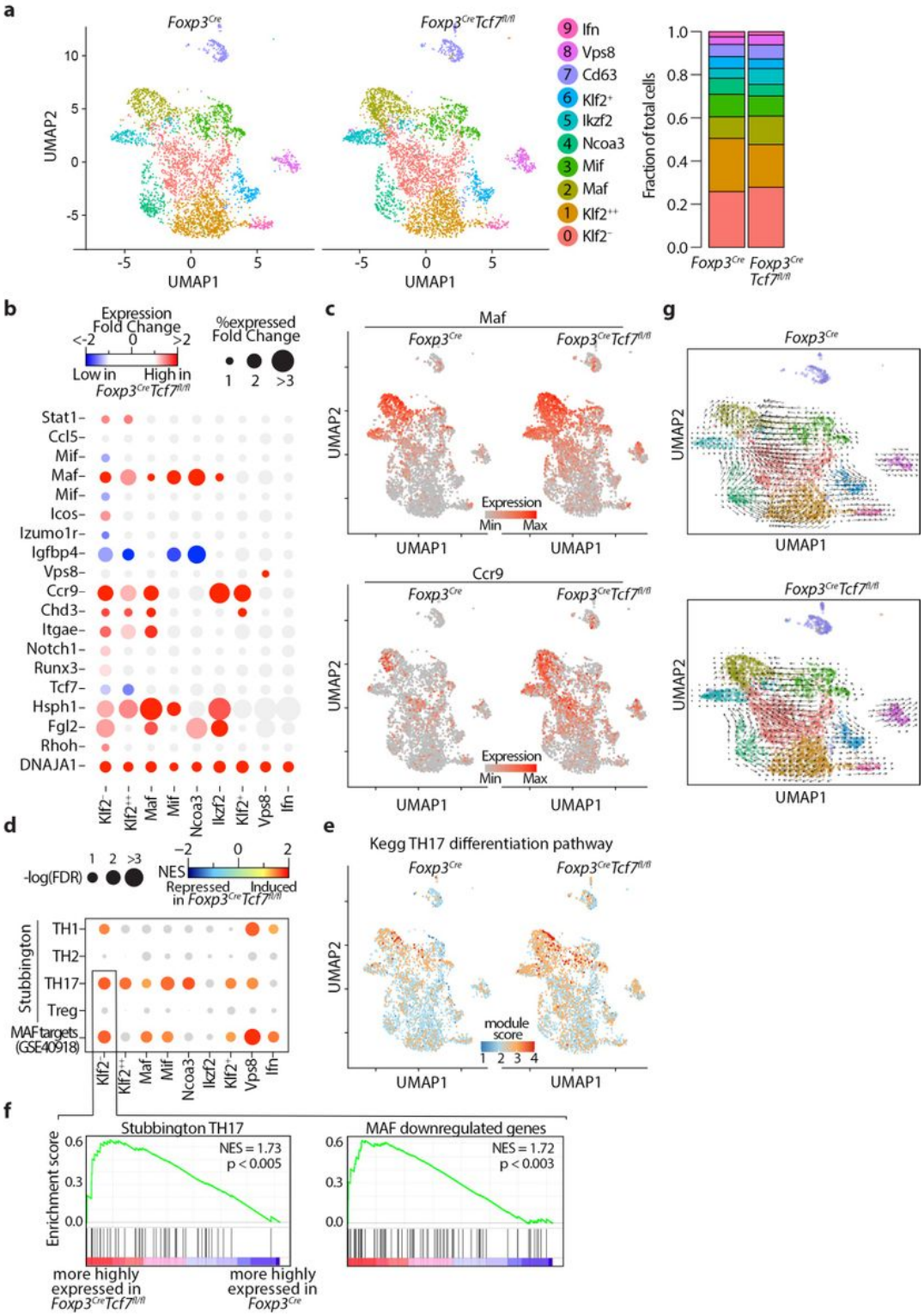

Figure 4

TCF1-deficient and sufficient Tregs show distinct effector functions. (a) UMAP projection (left) and fraction of cells in each cell type (stackbars; right panel) for TCF1-sufficient (Foxp3Cre) and TCF1-deficient (Foxp3Cre Tcf7fl/fl) Tregs. Data are from two replicates. (b) Expression changes of the most

differentially expressed genes between Tcf1-deficient and sufficient Tregs. See TableS3 for the full list. The fold change in expression intensities is color-coded. The fold change in percent of cells expressing the indicated gene in each cell type is proportional to the circle size. (c) Expression of Maf (top panel) and Ccr9 (bottom panel) projected on the UMAP. (d) GSEA analysis for the indicated gene lists comparing transcriptomes of Tcf1-sufficient and TCF1-deficient cells across all cell types. Normalized enrichment scores (NES) are color coded. log10 (FDR) values are proportional to the circle size. FDR>15% are masked with gray color. (e) Representative GSEA plots from “d” comparing TCF1-sufficient and TCF1-deficient Klf2– cells for Stubbington TH17 and MAF downregulated genes. (f) The UMAP projection of module scores for Kegg IL17 signalling pathway and related GSEA. (g) map showing observed (cells on the UMAP) and extrapolated future state of cells (overlaid arrows) based on RNA velocity for TCF1-sufficient (Foxp3Cre) and TCF1-deficient (Foxp3Cre Tcf7fl/fl) Tregs.

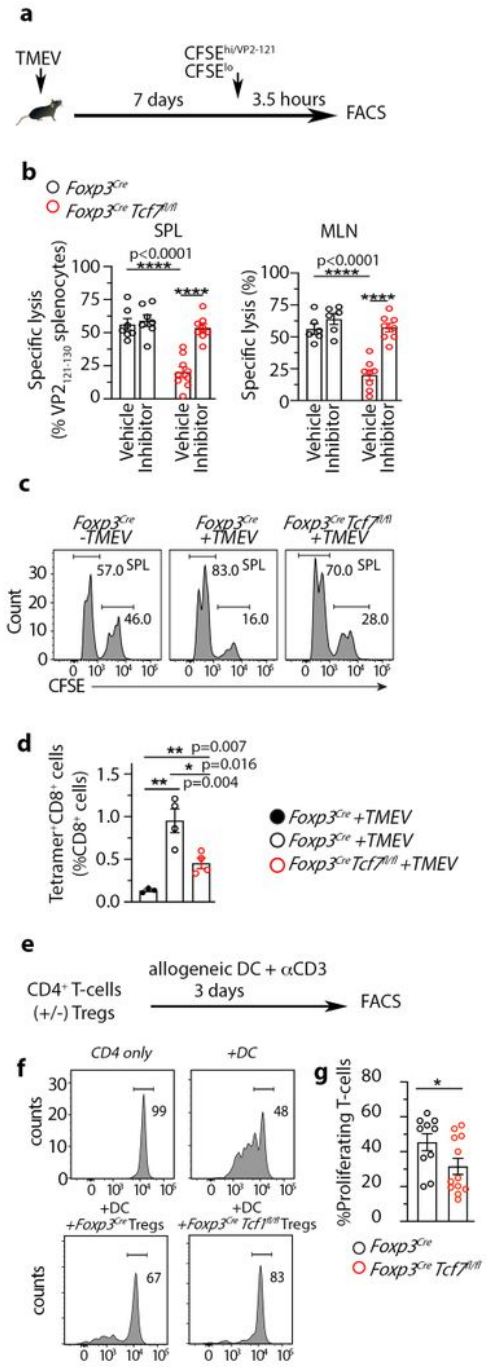

Figure 5

TCF1-deficient Tregs suppress viral antigen specific CD8+ T-cell cytotoxicity and T-cell proliferation. Foxp3CreTcf7fl/fl and control Foxp3Cre mice at 7-8 weeks of age (n = 6-9 per group) were compared for their antiviral T-cell response. (a) Schematic presentation of the in vivo kill assay. Mice were gavaged with vehicle or with the Tgfbrl small molecule inhibitor (LY3200882) twice daily starting from the day of viral infection. Specific in vivo kill of the VP2121-130 pulsed cells was measured by FACS four days after

transfer, based on the ratios of the two input cells after correction for cell death in adoptively transferred naïve mice. (b) Cumulative data quantified from specific lysis in spleen and MLN. (c) Representative FACS histograms of the same assay. (d) Tetramer analysis of VP2121-130 -specific CD8+ T-cells of the same assay. (e) Schematic presentation of CD4+ Tcell proliferation inhibition assay. T cells were purified from the spleen of C57B/6 mice, and Tregs fromFoxp3CreTcf7fl/fl mice and control Foxp3Cre mice at 5.5 months of age. FACS sorted CD4+CD25- cells were labelled with CFSE and incubated alone or with irradiated Balb/c DC, with or without equal numbers of Tregs.Dilution of CFSE by CD4 gated cells was measure after 3 days. (f) Representative FACS histograms of the same assay. (g) Cumulative data of percent of proliferating cells. Each symbol represents a value from an individual mouse. Data are means ± SEM (n = 4-8 per group). **** $p < 0.0001$, *** $p = 0.007$ or 0.004 as indicated, * $p = 0.016$ or <0.05 as indicated, Student's t test.

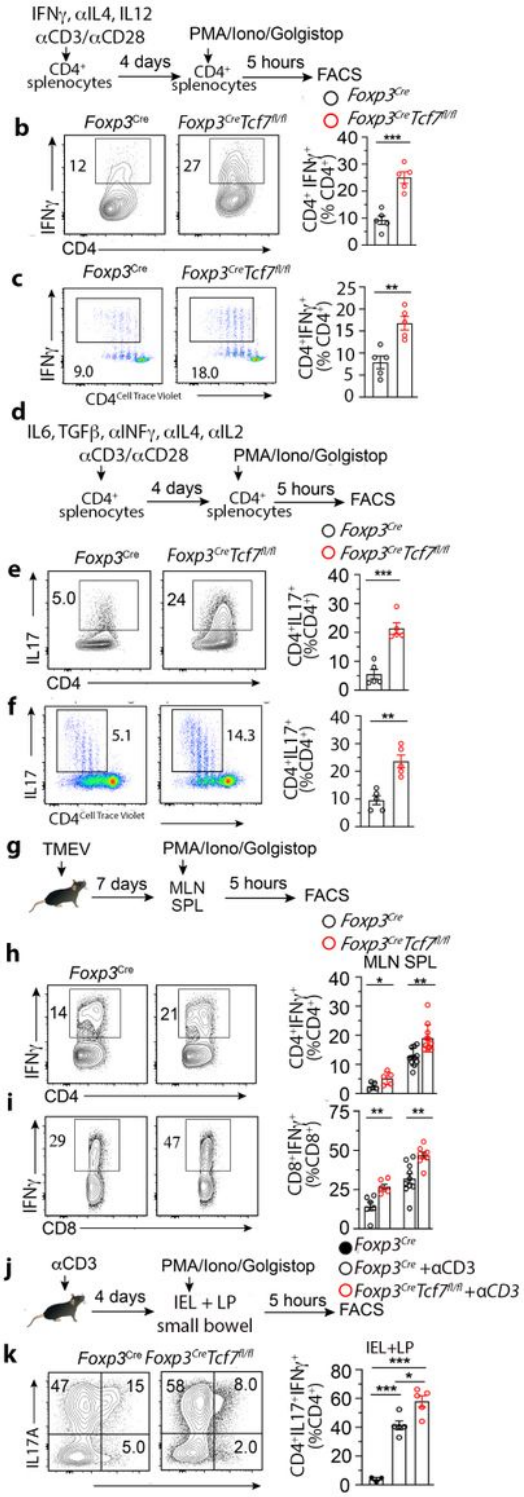

Figure 6

TCF1-deficient Tregs fail to suppress TH1 or TH17 polarization of CD4+ Tconv cells. Foxp3CreTcf7fl/f mice and control Foxp3Cre mice at 5.5 months of age (n = 5-8 per group) were used as source of Tregs for in vitro inhibition of T-helper cells polarization assays, or were used for in vivo assays. (a) Schematic presentation of in vitro TH1 polarization assay using spleen-derived CD4+ T-cells. (b) Total spleen CD4+ cells were magnetically purified from the indicated mice, in vitro stimulated for TH17 polarization for four

days and stained for intracellular Ifnγ. Representative FACS contour-plots (left) and cumulative histogram plots (right; n=5) are shown. (c) FACS purified 62L+CD44−CD25−CD45.1+CD4+ splenocytes were labelled with Cell Trace Violet, mixed 1:1 with YFP+CD45.2+CD4+CD25+ cells, and assayed for TH1 polarization as described. (d) Schematic presentation of in vitro TH17 polarizing assay using spleen-derived CD4+ T-cells. (e) CD4+ T-cells were purified as in “b” and after TH17 polarization were stained for intracellular IL17. (f) CD4+ T-cells and Tregs were purified and mixed as in “c” and after TH17 polarization were stained for intracellular IL17. (g) Schematic presentation of induction of in vivo TH1 response to TMEV, and FACS assay. (h) Representative FACS contourplots and cumulative histogram plots showing the extent of TH1 polarization of CD4+ T-cells as measured by expression of IFNγ. (i) The same for CD8+ T-cells. (j) Schematic presentation of induction of in vivo TH17 response, and FACS assay. (k) Representative FACS contour-plots and cumulative histogram plots showing the extent of TH17 polarization, measured by staining CD4+ T-cells for intracellular IL17. Each symbol in the cumulative data represents the value from an individual mouse. Data are means ± SEM (n = 5-8 per group). Statistical significance was determined by unpaired Student’s t-test. * $p < 0.05$; ** $p < 0.01$; *** $p< 0.001$, **** $p<0.0001$.

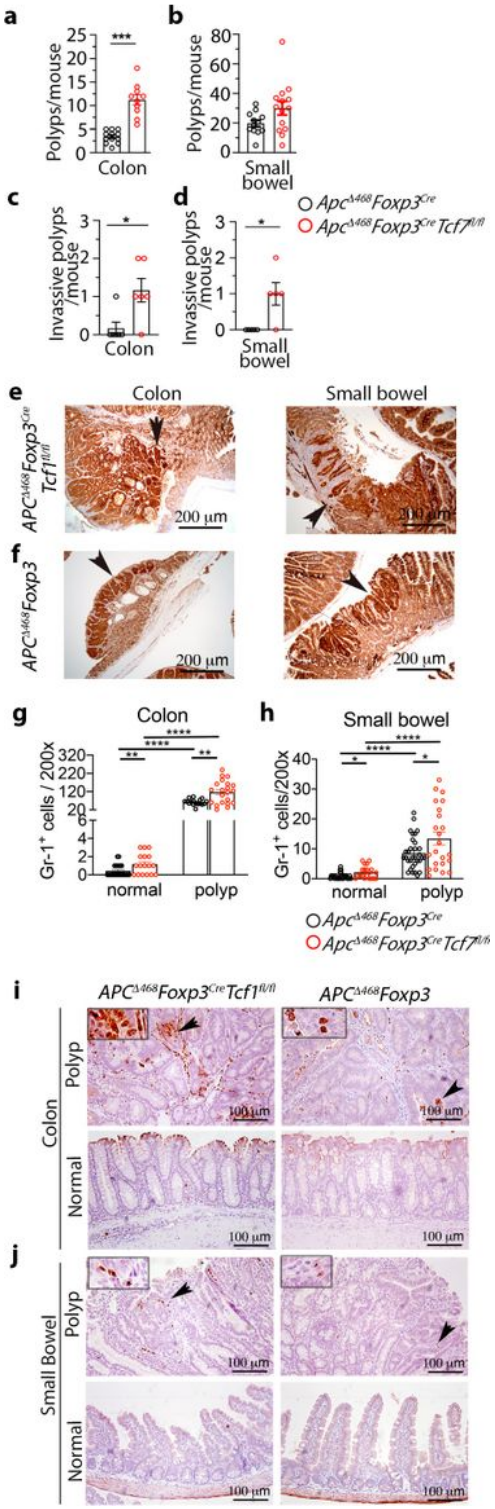

Figure 7

TCF1-deficient Tregs promote inflammation and tumor growth in polyposis-prone ApcD468 mice. ApcD468Foxp3CreTcf7fl/fl mice and control ApcD468Foxp3Cre mice were euthanized at 5.5 months of age. Polyp/tumor numbers were counted in the excised gut under a dissection microscope. Tumor aggression was evaluated by staining fixed tissues for b-catenin and counting lesions with extensive staining reaching the border of submucosa. (a) Polyp count in the colon, (b) polyp count in the small

bowel, (c) number of invasive lesions in the colon, (d) number of invasive lesions in the small bowel. Each symbol represents a value from an individual mouse. Tcf1-sufficient and deficient mice are represented by black and red symbols, respectively. (e) Representative immunohistochemistry stains of ApcD468Foxp3CreTcf7fl/fl mouse colon and small bowel for nuclear β-catenin. (f) The same for ApcD468Foxp3CreTcf7fl/fl mouse. (g) Quantification of Gr1 stained cells in colon polyps and distant healthy tissue. (h) The same in the small bowel. (i) Representative immunohistochemistry stains of mouse colon for Gr1. (j) The same for small bowel. Each symbol represents counts in one field of vision (FOV) at 200x, from a total of 4 mice per group. Statistical significance was determined by unpaired Student's t test. * $p < 0.05$; ** $p < 0.01$; *** $p < 0.001$, **** $p < 0.0001$.

Supplementary Files

This is a list of supplementary files associated with this preprint. Click to download.

- TableS1forFigure1.xlsx
- TableS2forFigure3.xlsx
- TableS3forFigure4.xlsx
- TableS4forFigureS5.xlsx